Hydrodynamic Modelling of Ria Formosa (South Coast of Portugal) with EcoDynamo

Pedro Duarte, Bruno Azevedo and António Pereira

University Fernando Pessoa, Centre for Modelling and Analysis of Environmental Systems

January 2005

DITTY (Development of an information technology tool for the management of Southern European lagoons under the influence of river-basin runoff)

(EESD Project EVK3-CT-2002-00084)

Summary

In this work a hydrodynamic model of Ria Formosa (South of Portugal) is presented. Ria Formosa is a large (c.a. 100 km2) mesotidal lagunary system with large intertidal areas and several conflicting uses, such as fisheries, aquaculture, tourism and nature conservation. This coastal ecosystem is a natural park where several management plans and administrative responsibilities overlap.

The work presented here is part of a coupled hydrodynamic-biogeochemical model that includes pelagic and benthic processes and variables. It is a two-dimensional vertically integrated hydrodynamic model, based on a finite differences grid with a 100 m spatial step and a semi-implicit resolution scheme. It is forced by tide level changes at the sea boundary and river flows at the land boundary. The model includes a wet-drying scheme to account for the dynamics of the large intertidal areas.

The purposes of this work are to: (i) describe the model; (ii) present its calibration and validation against field data; (iii) use the model to analyse circulation patterns and estimate the water residence time and (iv) analyse the dispersion of effluents rejected by the Waste Water Treatment Plants located in the lagoon.

CONTENTS

1 Introduction

This work is part of the DITTY project "Development of an Information Technology Tool for the Management of European Southern Lagoons under the influence of river-basin runoff" (http://www.dittyproject.org/). The general objective of this project is the development of information technology tools integrating Databases, Geographical Information Systems (GIS), Mathematical Models and Decision Support Systems to help in the management of southern European coastal lagoons and adjacent watersheds, within the spirit of the Water Framework Directive (UE, 2000).

The DITTY project takes place in five southern European coastal lagoons. The work presented here concerns the hydrodynamic modelling of Ria Formosa – the Portuguese case study within DITTY (Fig. 1-1). The coupling of this model with a biogeochemical model including water and sediment processes will be the subject of an upcoming report.

1.1 Site description

Ria Formosa is a shallow mesotidal lagoon located at the south of Portugal (Algarve coast) with a wet area of 10 500 ha (Figure 1-1). The lagoon has several channels and a large intertidal area, which corresponds roughly to 50% of the total area, mostly covered by sand, muddy sand-flats and salt marshes. The intertidal area is exposed to the atmosphere for several hours, over each semi-diurnal tidal period, due to its gentle slopes. Fresh water input to the lagoon is negligible and salinity remains close to 36 ppt, except during sporadic and short periods of winter run-off. The tidal amplitude varies from 1 to 3.5 meters and the mean water depth is 3.5 m. There is a rather intense exchange of 50 – 75% of water mass during each tide (Falcão et al., 2003).

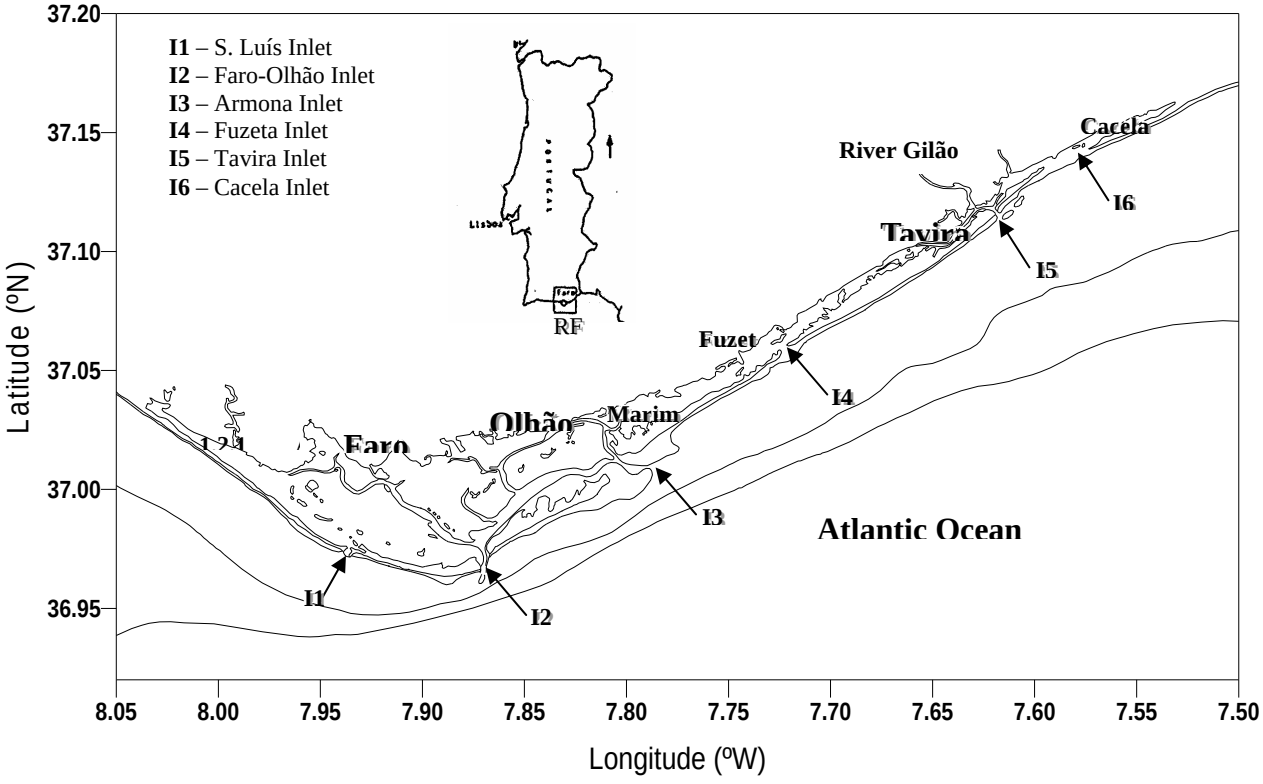

Figure 1-1- Geographic location of Ria Formosa and its inlets (I1 – I6).

1.2 Objectives

The objectives of this report are to:

i. Describe the model and how it was implemented, giving details on numerical methods and software developed

ii. Describe model calibration and validation

iii. Use the model to analyse general circulation patterns and estimate water residence times

iv. Use the model to analyse the dispersion of effluents rejected by the Waste Water Treatment Plants (WWTP) located in Ria Formosa.

2 Methodology

2.1 Model description

The hydrodynamic model implemented in this work is a two dimensional solution of the Navier-Stocks equations adapted from Neves (1985). It is based on a finite difference staggered grid (Vreugdenhil, 1989). Flows are solved at the sides of the grid cells, whereas surface elevations and concentrations are calculated at the center of the cells. Advection terms are calculated using an upwind scheme, whereas diffusion terms are based on a central differences scheme (see below). The resolution is semi-implicit. At the first semi time step the u component is solved implicitly and the v component solved explicitly. At the second semi time step it is the other way around. After the calculation of both velocity components, surface elevation is calculated by continuity, as well as the concentration of conservative and non-conservative substances, after solving for the sources and sinks. The model is forced by tidal height at the sea boundaries. It can also be forced by wind and fresh water flows.

Equation of Continuity

$$\frac{\xi_{ij}^{n+\frac{1}{2}} - \xi_{ij}^{n}}{\Delta t/2} + \frac{1}{2\Delta x}\left[\left(H_{lJ} + H_{lJ+1}\right)u_{ij+1} - \left(H_{ij} + H_{ij-1}\right)u_{ij}\right]^{n+\frac{1}{2}} + \frac{1}{2\Delta x}\left[\left(H_{ij} + H_{i+1j}\right)v_{i+1j} - \left(H_{ij} + H_{i-1j}\right)v_{ij}\right]^{n} = 0 \quad \textbf{(1)}$$

ξ - Surface elevation (m)

Δx - Spatial step (100 m)

H - Depth (m)

u and v - Current speed (East-West and North- South, respectively) (m s^{-1})

n and $n+\frac{1}{2}$ - Terms at the beginning and at the final of the first semi time step

At the second semi time step the u terms are reported to time $n+\frac{1}{2}$ and the v terms are reported to time n.

Equation for the u ***component at the first semi time step***

The second and third terms on the left side of the equation are the advection components, the first term on the right side is the barotropic pressure gradient acceleration, the second term corresponds to drag, the third term is the Coriolis acceleration and the fourth term corresponds to momentum transfer by diffusion.

$$\frac{u_{ij}^{n+1/2}-u_{ij}^{n}}{\Delta t/2}+\frac{1}{(H_{ij}+H_{ij-1})}\left[\begin{array}{l}\dfrac{H_{ij}\left(u_{ij+1/2}+\left|u_{ij+1/2}\right|\right)u_{ij}}{\Delta x}-\dfrac{H_{ij-1}\left(u_{ij-1/2}+\left|u_{ij-1/2}\right|\right)u_{ij-1}}{\Delta x}+\\ \dfrac{H_{ij}\left(u_{ij+1/2}-\left|u_{ij+1/2}\right|\right)u_{ij+1}}{\Delta x}-\dfrac{H_{ij-1}\left(u_{ij-1/2}-\left|u_{ij-1/2}\right|\right)u_{ij}}{\Delta x}\end{array}\right]^{n+1/2}+$$

$$+\frac{1}{(H_{ij}+H_{ij-1})}\left[\begin{array}{l}\dfrac{H_{i+1/2j-1/2}\left(v_{i+1/2j-1/2}+\left|v_{i+1/2j-1/2}\right|\right)u_{ij}}{\Delta x}-\dfrac{H_{i-1/2j-1/2}\left(v_{i-1/2j-1/2}+\left|v_{i-1/2j-1/2}\right|\right)u_{i-1j}}{\Delta x}+\\ \dfrac{H_{i+1/2j-1/2}\left(v_{i+1/2j-1/2}-\left|v_{i+1/2j-1/2}\right|\right)u_{i+1j}}{\Delta x}-\dfrac{H_{i-1/2j-1/2}\left(v_{i-1/2j-1/2}-\left|v_{i-1/2j-1/2}\right|\right)u_{ij}}{\Delta x}\end{array}\right]^{n}=$$

$$=-g\frac{\xi_{ij}^{n+1/2}-\xi_{ij-1}^{n+1/2}}{\Delta x}-\frac{1}{(H_{ij}+H_{ij-1})}(Cf_{ij}+Cf_{ij-1})\|u\|u_{ij}^{n+1/2}+$$

$$\frac{1}{4}f(v_{ij-1}+v_{ij-1}+v_{i+1j-1}+v_{i+1j})^{n+1/2}+ \qquad \textbf{(2)}$$

$$\frac{\nu}{\Delta x^{2}}\left[(u_{ij+1}+u_{ij-1}-2u_{ij})^{n+1/2}+(u_{i+1j}+u_{i-1j}-2u_{ij})^{n}\right]$$

Where,

g - Acceleration of gravity (m s^{-2})

ν - Coefficient of eddy diffusion ($m^2 s^{-1}$)

f - Coriolis parameter (s^{-1})

Equation for the v component at the first semi time step

All terms are presented in the same order as for the u component (see above).

$$v_{ij}^{n+1/2} = v_{ij}^{n} - \frac{\Delta t}{2(H_{ij}+H_{i-1j})}\left[\begin{array}{l}\dfrac{H_{ij}\left(v_{i+1/2j}+\left|v_{i+1/2j}\right|\right)v_{ij}}{\Delta x} - \dfrac{H_{i-1j}\left(v_{i-1/2j}+\left|v_{i-1/2j}\right|\right)v_{i-1j}}{\Delta x} + \\ \dfrac{H_{ij}\left(v_{i+1/2j}-\left|v_{i+1/2j}\right|\right)v_{i+1j}}{\Delta x} - \dfrac{H_{i-1j}\left(v_{i-1/2j}-\left|v_{i-1/2j}\right|\right)v_{ij}}{\Delta x}\end{array}\right]^{n} -$$

$$\frac{\Delta t}{2(H_{ij}+H_{i-1j})}\left[\begin{array}{l}\dfrac{H_{i-1/2j+1/2}\left(u_{i-1/2j+1/2}+\left|u_{i-1/2j+1/2}\right|\right)v_{ij}}{\Delta x} - \dfrac{H_{i-1/2j-1/2}\left(u_{i-1/2j-1/2}+\left|u_{i-1/2j-1/2}\right|\right)v_{ij-1}}{\Delta x} - \\ \dfrac{H_{i-1/2j+1/2}\left(u_{i-1/2j+1/2}-\left|u_{i-1/2j+1/2}\right|\right)v_{ij+1}}{\Delta x} - \dfrac{H_{i-1/2j-1/2}\left(u_{i-1/2j-1/2}-\left|u_{i-1/2j-1/2}\right|\right)v_{ij}}{\Delta x}\end{array}\right]^{n} -$$

$$\frac{\Delta t}{2} g \frac{\xi_{ij}^{n} - \xi_{i-1j}^{n}}{\Delta x} - \frac{\Delta t}{2(H_{ij}+H_{i-1j})}(Cf_{ij}+Cf_{i-1j})\|v\|v_{ij} + \frac{\Delta t}{8} f(u_{ij}+u_{ij+1}+u_{i-1j}+u_{i-1j+1})^{n} +$$

$$\frac{\nu \Delta t}{2\Delta x^{2}}\left[(v_{i+1j}+v_{i-1j}-2v_{ij})^{n} + (v_{ij+1}+v_{ij-1}-2v_{ij})^{n}\right]$$

(2)

Equation 1 is used to substitute the ξ terms in equations 2 and 3. At the first semi time step (2) is solved implicitly and (3) is solved explicitly. To solve (1) implicitly it is necessary to rearrange the equation, in order to separate the $n+\frac{1}{2}$ to the left side and the n to the right side of it. An implicit solution may be achieved by solving the equation in the general form:

$$b_{1ij}u_{ij-1}^{n+1/2} + b_{2ij}u_{ij}^{n+1/2} + b_{3ij}u_{ij+1}^{n+1/2} = d_{ij} \qquad \textbf{(4)}$$

Where the terms b_{1ij}, b_{2ij}, b_{3ij} and d_{ij} are:

$$b_{1ij} = -\frac{\Delta t}{2(H_{ij} + H_{ij-1})} \frac{H_{ij-1}\left(u_{ij-1/2} + \left|u_{ij-1/2}\right|\right)}{\Delta x} - \frac{\nu}{\Delta x^2}\frac{\Delta t}{2} - \frac{g\left(H_{ij-1} + H_{ij-2}\right)\Delta t^2}{8\Delta x^2} \quad \textbf{(5)}$$

$$b_{2ij} = 1 + \frac{\Delta t}{2(H_{ij} + H_{ij-1})}\left(\frac{H_{ij-1}\left(u_{ij+1/2} + \left|u_{ij+1/2}\right|\right)}{\Delta x} - \frac{H_{ij-1}\left(u_{ij-1/2} - \left|u_{ij-1/2}\right|\right)}{\Delta x}\right) + \frac{(Cf_{ij} + Cf_{ij-1})\|u\|}{} \quad \textbf{(6)}$$

$$\frac{\nu\Delta t}{\Delta x^2} + \frac{g\left(H_{ij} + H_{ij-1}\right)\Delta t^2}{4\Delta x^2}$$

$$b_{3ij} = \frac{\Delta t}{2(H_{ij} + H_{ij-1})} \frac{H_{ij}\left(u_{ij+1/2} - \left|u_{ij+1/2}\right|\right)}{\Delta x} - \frac{\nu}{\Delta x^2}\frac{\Delta t}{2} - \frac{g\left(H_{ij} + H_{ij+1}\right)\Delta t^2}{8\Delta x^2} \quad \textbf{(7)}$$

$$d_{ij} = u_{ij}^n + \frac{1}{8}\Delta t F(v_{ij} + v_{ij-1} + v_{i+1j-1} + v_{i+1j})^{n+1/2} + \frac{\Delta t}{2}\frac{\nu}{\Delta x^2}(u_{i+1j} + u_{i-1j} - 2u_{ij})^n -$$

$$\frac{\Delta t}{(H_{ij} + H_{ij-1})}\left[\begin{array}{l} \frac{H_{i+1/2j-1/2}\left(v_{i+1/2j-1/2} + \left|v_{i+1/2j-1/2}\right|\right)u_{ij}}{\Delta x} - \\ \frac{H_{i-1/2j-1/2}\left(v_{i-1/2j-1/2} + \left|v_{i-1/2j-1/2}\right|\right)u_{i-1j}}{\Delta x} + \\ \frac{H_{i+1/2j-1/2}\left(v_{i+1/2j-1/2} - \left|v_{i+1/2j-1/2}\right|\right)u_{i+1j}}{\Delta x} - \\ \frac{H_{i-1/2j-1/2}\left(v_{i-1/2j-1/2} - \left|v_{i-1/2j-1/2}\right|\right)u_{ij}}{\Delta x} \end{array}\right]^n - \quad \textbf{(8)}$$

$$-\frac{g\xi_{ij}^n\Delta t}{2\Delta x} - \frac{g\Delta t^2(-H_{ij}v_{i+1j}^n - H_{i+1j}v_{i+1j}^n + H_{ij}v_{ij}^n + H_{i-1j}v_{ij}^n)}{8\Delta x^2} +$$

$$+\frac{g\xi_{ij}^n\Delta t}{2\Delta x} + \frac{g\Delta t^2(-H_{ij-1}v_{i+1j-1}^n - H_{i+1j-1}v_{i+1j-1}^n + H_{ij-1}v_{ij-1}^n + H_{i-1j-1}v_{ij-1}^n)}{8\Delta x^2}$$

Equation (4) changes at the boundaries. At ocean boundaries water elevation is determined by tidal forcing. Therefore, at eastern ocean boundaries equation (4) becomes:

$$b_{2ij}u_{ij}^{n+1/2} + b_{3ij}u_{ij+1}^{n+1/2} = d_{ij} - b_{1ij}u_{ij-1}^{n+1/2} \qquad \textbf{(9)}$$

With $\xi_{ij-1}^{n+\frac{1}{2}}$ a boundary condition, the u_{ij-1} component across the boundary is determined by continuity:

$$u_{ij-1} = \begin{bmatrix} 2\Delta x\xi_{ij-1}^{n+\frac{1}{2}} + 0.5\Delta t\left(H_{ij-1} + H_{ij}\right)u_{ij}^{n+\frac{1}{2}} - \\ 2\Delta x\xi_{ij-1}^{n} + 0.5\Delta t\left(H_{ij-1} + H_{i+1j-1}\right)v_{i+1j-1}^{n} - \\ 0.5\Delta t\left(H_{ij-1} + H_{i-1j-1}\right)v_{ij-1}^{n} \end{bmatrix}^{n+\frac{1}{2}} / \left[0.5\Delta t\left(H_{ij-1} + H_{ij-1}\right)\right] \qquad \textbf{(10)}$$

Replacing u_{ij-1} in (9) with (10) and solving, b_{1ij} becomes:

$$b_{1ij} = -\frac{\Delta t}{2(H_{ij} + H_{ij-1})}\frac{H_{ij-1}\left(u_{ij-1/2} + \left|u_{ij-1/2}\right|\right)}{\Delta x} - \frac{\nu}{\Delta x^2}\frac{\Delta t}{2} - \frac{gH_{ij-1}\Delta t^2}{\Delta x^2} \qquad \textbf{(11)}$$

At western ocean boundaries and following a similar reasoning, b_{3ij} becomes:

$$b_{3ij} = \frac{\Delta t}{2(H_{ij} + H_{ij-1})}\frac{H_{ij}\left(u_{ij+1/2} - \left|u_{ij+1/2}\right|\right)}{\Delta x} - \frac{\nu}{\Delta x^2}\frac{\Delta t}{2} - \frac{gH_{ij}\Delta t^2}{4\Delta x^2} \qquad \textbf{(12)}$$

Regarding the v component, at the second semi time step, the rationale is the same in a north-south direction.

At western or eastern land boundaries, the velocity component perpendicular to land is assumed to be zero. At river boundaries, the velocity component parallel to the river is determined by river flow.

To solve implicitly for $u_{ij}^{n+1/2}$ (in the first semi time step) or $v_{ij}^{n+1/2}$ (in the second semi time step) it is necessary to invert the matrix of the b terms. The routine tridag (Press et al., 1995) is used for this purpose. At each time step, after solving for $u_{ij}^{n+1/2}$ and $v_{ij}^{n+1/2}$, the surface elevations are updated with (1).

At the end of each time step the transport equation is solved for all water column dissolved and suspended variables and temperature:

$$(HS)_{ij}^{n+\frac{1}{2}} = \begin{bmatrix} \left(0.5\Delta t\left(H_{ij}+H_{ij-1}\right)S_{ij-1}\right)u_{ij}^{n+\frac{1}{2}} - \left(0.5\Delta t\left(H_{ij}+H_{ij+1}\right)S_{ij}\right)u_{ij+1}^{n+\frac{1}{2}} + \\ 2\Delta x(HS)_{ij}^{n} - \\ \left(0.5\Delta t\left(H_{ij}+H_{ij+1}\right)S_{ij}\right)v_{i+1j}^{n} + \left(0.5\Delta t\left(H_{ij}+H_{i-1j}\right)S_{i-1j}\right)v_{ij}^{n} \end{bmatrix} / 2\Delta x + \\ \begin{bmatrix} \frac{0.5\Delta t\nu\left(H_{ij+1}+H_{ij}\right)S_{ij+1} - 0.5\Delta t\nu\left(H_{ij+1}+H_{ij}\right)S_{ij}}{2\Delta x^2} - \\ \frac{0.5\Delta t\nu\left(H_{ij}+H_{ij-1}\right)S_{ij} - 0.5\Delta t\nu\left(H_{ij}+H_{ij-1}\right)S_{ij-1}}{2\Delta x^2} + \\ \frac{0.5\Delta t\nu\left(H_{i+1j}+H_{ij}\right)S_{i+1j} - 0.5\Delta t\nu\left(H_{i+1j}+H_{ij}\right)S_{ij}}{2\Delta x^2} - \\ \frac{0.5\Delta t\nu\left(H_{ij}+H_{i-1j}\right)S_{ij} - 0.5\Delta t\nu\left(H_{ij}+H_{i-1j}\right)S_{i-1j}}{2\Delta x^2} \end{bmatrix} \quad \textbf{(13)}$$

Where S represents the concentration of any conservative or non-conservative variable. At the second semi time step the u terms are reported to time $n+\frac{1}{2}$ and the v terms are reported to time n.

The model grid has 282 lines and 470 columns. Each cell is 100 X 100 m. The bathymetry was obtained from a bathymetric survey carried out by the Portuguese Hydrographic Institute in 2000 and is presented in Fig 2-2.

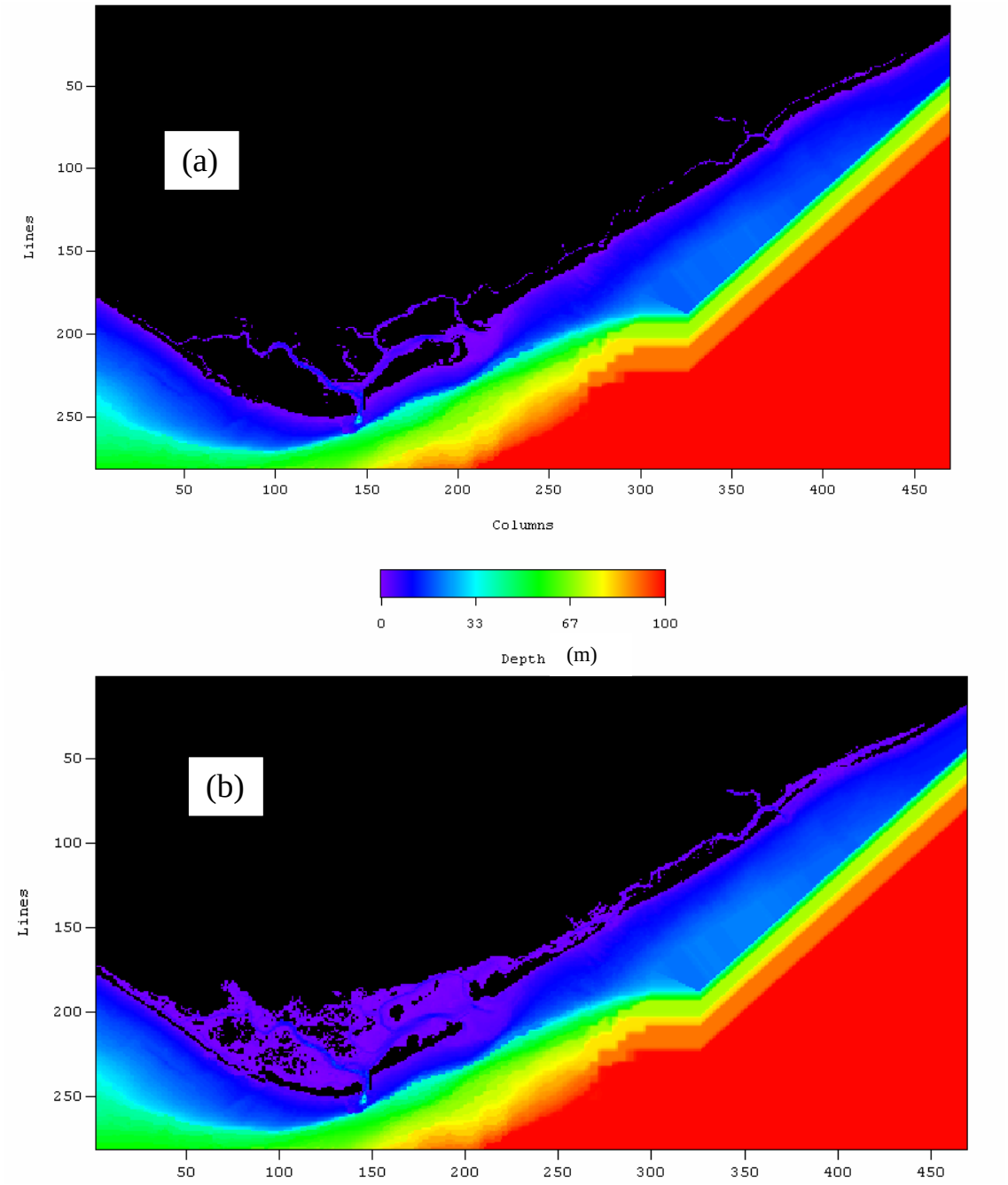

Fig. 2-2 – Model bathymetry (282 lines X 470 columns, each with 100 X 100 m), reported to the hydrographic zero (a) and during a flood (b) (tide level = 2.6 m).

Given the large intertidal areas of Ria Formosa (cf. – 1.1), the model includes a wet-drying scheme that prevents any grid cell from running completely dry, avoiding numerical errors. The general approach is to stop using the advection term when depth is lower than a threshold value (0.1 m in the present case) to avoid numerical instabilities. Below this threshold and until a minimum limit of 0.05 m, the model computes all remaining terms. When this limit is reached, computations do not take

place in a given cell until a neighbour cell has a higher water level, allowing then the pressure term to start “filling” the “dry” cell.

This model is forced by water level at sea boundaries and river discharges at land boundaries. The former are calculated by the equations and the harmonic components for the Faro-Olhão harbour (cf. – Fig.1-1) described in SHOM (1984) and listed in Table 2-1. Regarding the latter, only River Gilão (Fig. 1-1) was considered in the simulations described in this report, with a flow of 30 m^3s^{-1} (winter flow estimated from rainfall).

Table 2-1 – Mean water level and harmonic constants for the Faro-Olhão harbour according to SHOM(1984).

Mean level	Z0	2000	mm	
			Amplitude in mm	Phase in degrees
Harmonic constants	10	Sa	0	0
		Q1	0	0
		O1	60	331
		K1	60	69
		N2	190	78
		M2	930	94
		S2	320	125
		MN4	0	0
		M4	40	150
		MS4	20	162

2.2 Model implementation

The model was implemented with EcoDynamo (Pereira & Duarte, 2005) - an object-oriented modelling software written in C++. There are different objects to simulate hydrodynamic, thermodynamic and biogeochemical processes and variables. The shell interface (Fig. 2-3) allows the user to choose among different models and to define the respective setups – time steps, output formats (file, graphic and tables), objects to be used and variables to be visualised. The list of objects, variables and parameters of model equations are stored in specific files. Objects may communicate among them for data exchange. In the present work two objects are used – one to simulate the hydrodynamic equations described above and a tide object to simulate water level at the sea boundaries (cf. – 2.2).

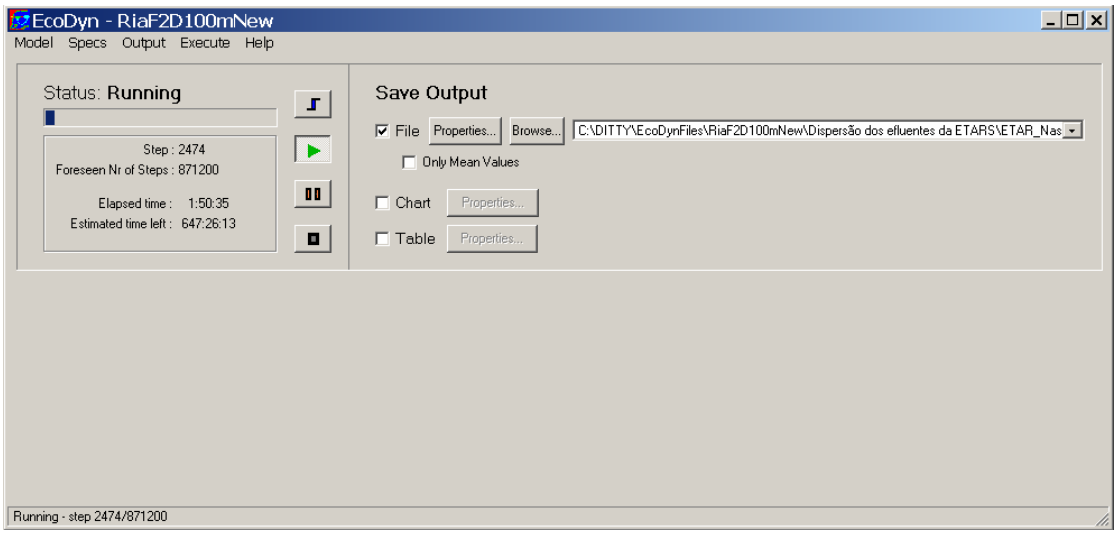

Fig. 2-3 – EcoDynamo interface.

2.3 Model calibration and validation

Model calibration and validation was based on current velocity and tide gauge data collected by the Portuguese Hydrographic Institute in 2001(IH, 2001) at a number of stations (Fig. 2-4), over periods of several days (not necessarily coincident among different stations), between January and March 2001. Ideally, two independent data sets should have been used – one for calibration and another for validation. However, since there was only one dataset available and since the model reproduced observed data relatively well, without any calibration effort (see below), calibration and validation are here considered together. Furthermore, changing model parameters locally, such as turbulent diffusivity or bottom drag, seeking for a better model fit to observed data, would hardly be consistent in future simulations, in a system where bottom configuration and bathymetry changes so rapidly. Therefore, efforts were mostly directed towards a rigorous bathymetric description and the determination of the accurate position of all inlets at the time when sampling surveys were carried out.

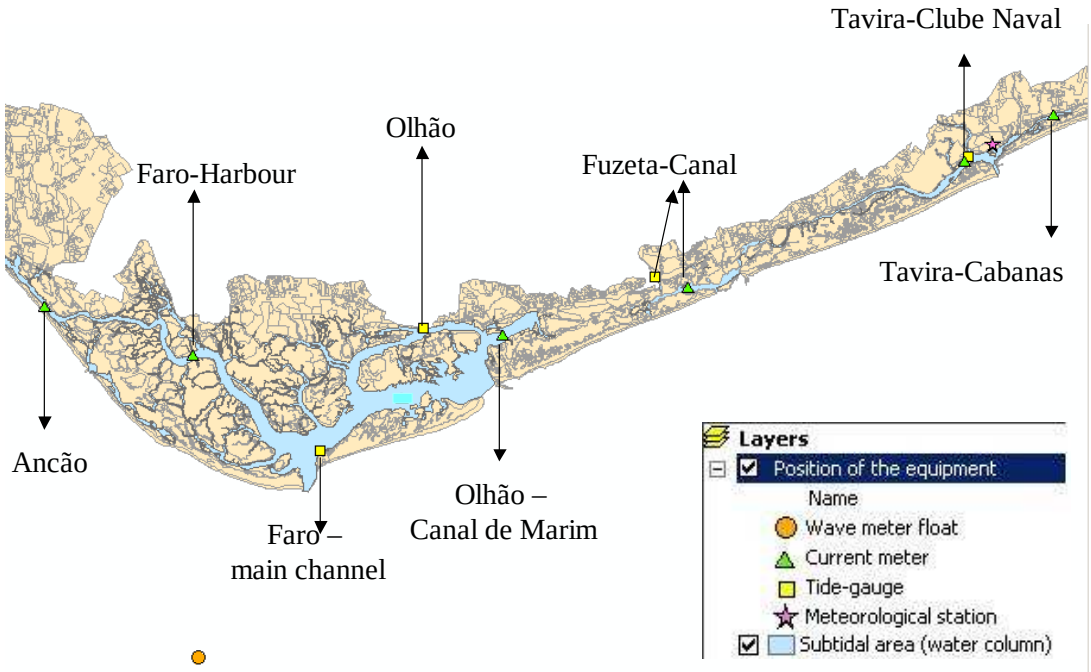

Fig. 2-4 – GIS image showing the location of current meter and tide-gauge stations surveyed by the Portuguese Hydrographic Institute in 2001 (IH, 2001) and used for model calibration (see text).

Model simulations were carried out for the same period over which current velocity and tide gauge measurements were available (January 2001 -). The same time period was used for all simulations described in this report (see below).

The overall correspondence between observed and predicted values was analysed with Model II linear regression analysis, following Laws and Archie (1981), with the major axis regression method as recommended by Mesplé et al. (1996) and described in Sokal and Rohlf (1995). ANOVA was used to test the significance of slopes and y-intercepts obtained, including the variance explained by the model. When the slope is not significantly different (s.d.) from one and the y-intercept not s.d. from zero, there is a good agreement between model and observations. When the y-intercept is s.d. from zero, there is a constant difference between model and observations. When the slope is s.d. from one but s.d. from zero, the differences between model and observations are proportional to the value of the variable. Howerver, the model may still explain a significant proportion of total variance.

2.4 Analysis of general circulation patterns and residence times

Simulations were carried out to analyse general circulation patterns and to estimate water residence time (WRT). The former were analysed through vector plots. WRT was estimated by "filling" the lagoon with salt water and the ocean with fresh water and running the model until the lagoon water was "washed" to the sea.

Simulation results were used to calculate input, output and residual flows across Ria Formosa inlets (see Fig. 1-1) in order to get an overall picture of lagoon circulation and the relative importance of the different inlets.

2.5 Dilution of effluents from Waste Water Treatment Plants

There are several WWTPs inside the limits of the Ria Formosa Natural Park (RFNP), discharging their effluents into the lagoon waters. The geographical distribution of the WWTPs is shown in Fig. 2-5.

In order to evaluate the dispersion patterns of the effluents from WWTPs, a conservative tracer was discharged as an effluent from each WWTP (only one WWTP was considered in each simulation). The discharge occurred for the first six hours of the first simulation day. A total of 140 hours were simulated. The tracer dispersion and concentration decrease were later analysed.

The types of land cover in the surroundings of the WWTPs were also analysed in a GIS, in order to evaluate the most sensible areas such as salt ponds, fish ponds or shellfish farming areas.

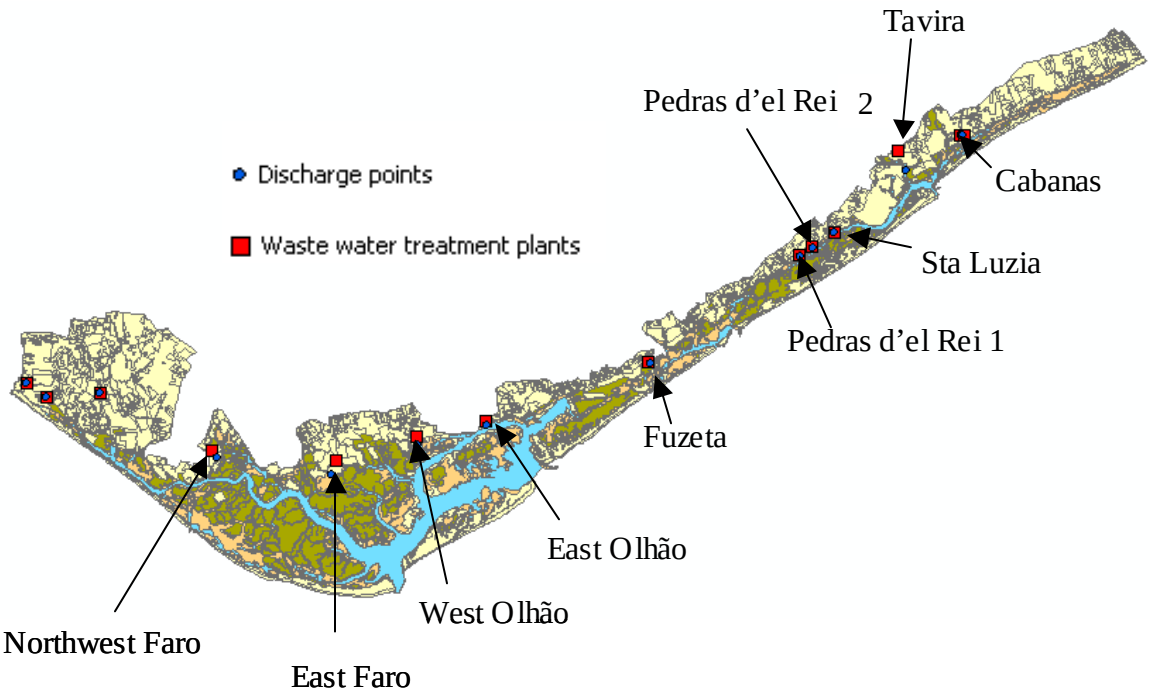

Fig. 2-5 – Present location of Waste Water Treatment Plants in Ria Formosa (see text).

3 Results and Discussion

3.1 Model calibration and validation

In the next figures, measured and predicted current velocities (Figs. 3-1 – 3-6) and water levels (Figs. 3-7 – 3-10) are shown for each of the monitoring locations depicted in Fig. 2-4. Regarding both current velocities and water levels, the visual fit between measurements and observations is generally good, except for current velocities at stations Tavira-Cabanas and Tavira-Clube Naval (Figs. 3-5 and 3-6).

Current speeds range from nearly zero till values in excess of 100 cm s^{-1}. Velocity peaks occur both at the middle of the ebb and the middle of the flood. This is a normal phenomena in inlets - when current switches from flood to ebb, the water level is near its peak flood value (Militello & Hughes, 2000).

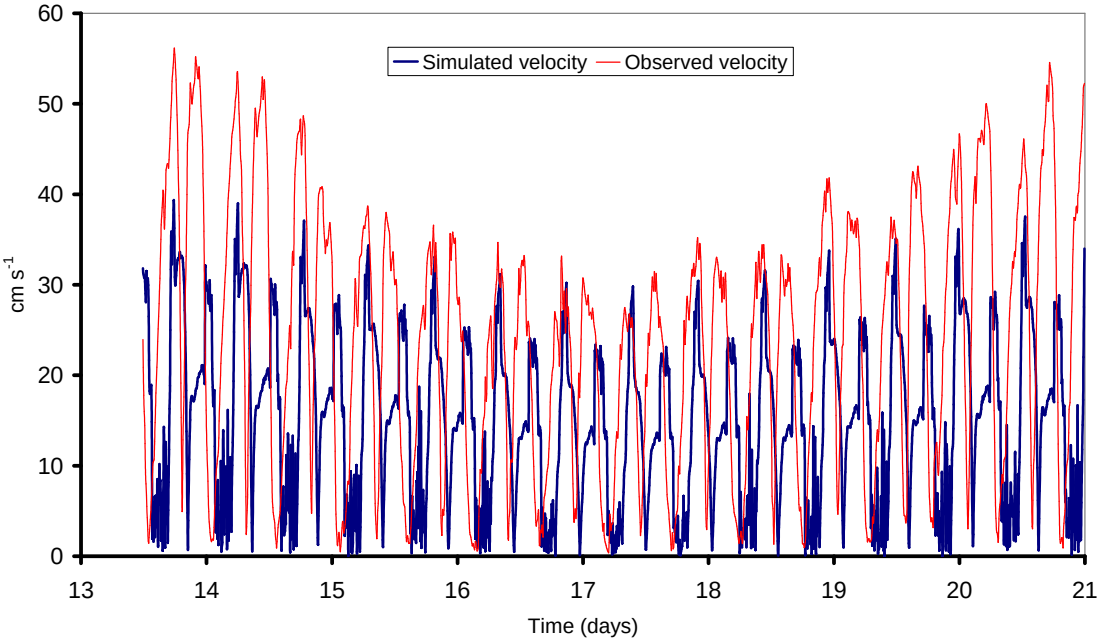

Fig. 3-1 – Predicted and measured velocities at Ancão (cf. – Fig. 2-4) (see text).

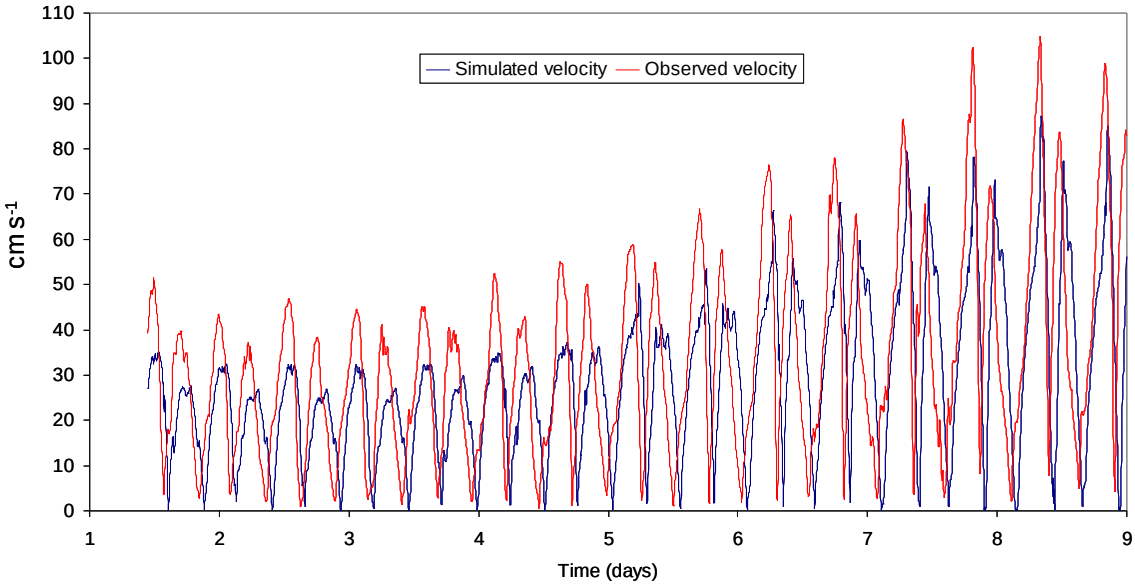

Fig. 3-2 – Predicted and measured velocities at Olhão – Canal de Marim (cf. – Fig. 2-4).

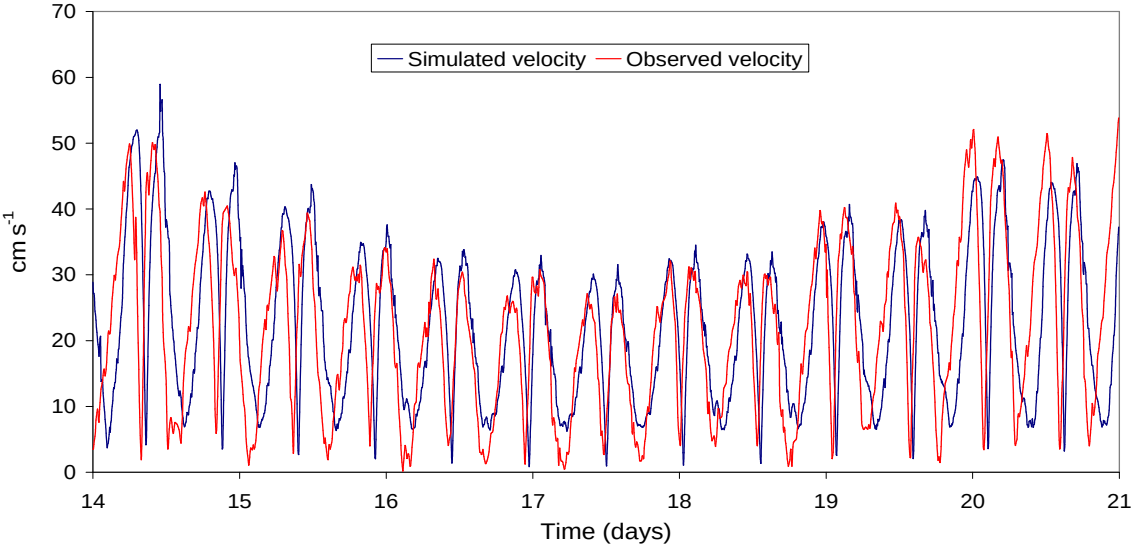

Fig. 3-3 – Predicted and measured velocities at Faro-Harbour (cf. – Fig. 2-4).

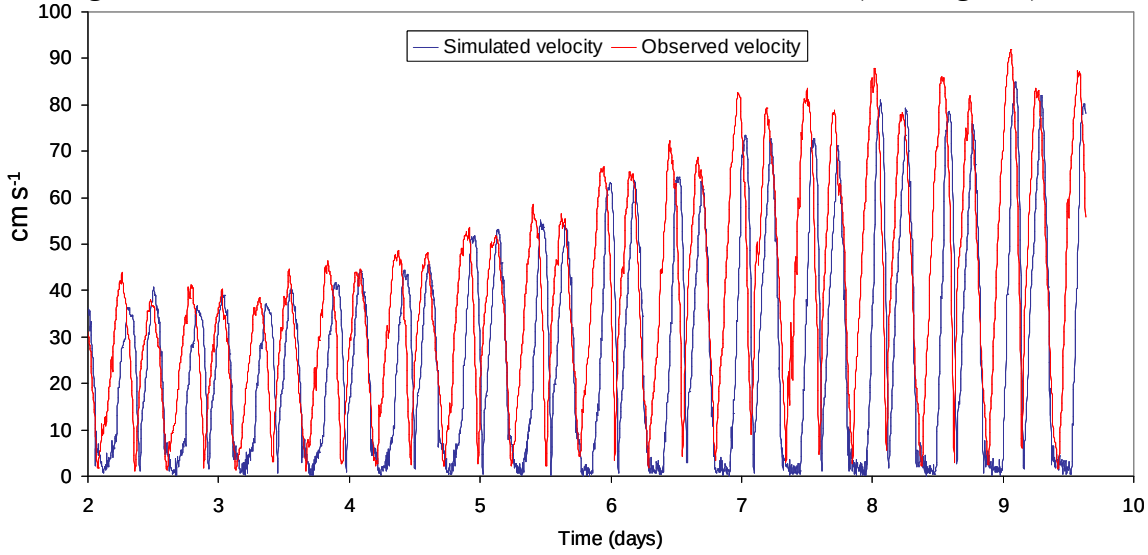

Fig. 3-4 – Predicted and measured velocities at Fuzeta - Canal (cf. – Fig. 2-4).

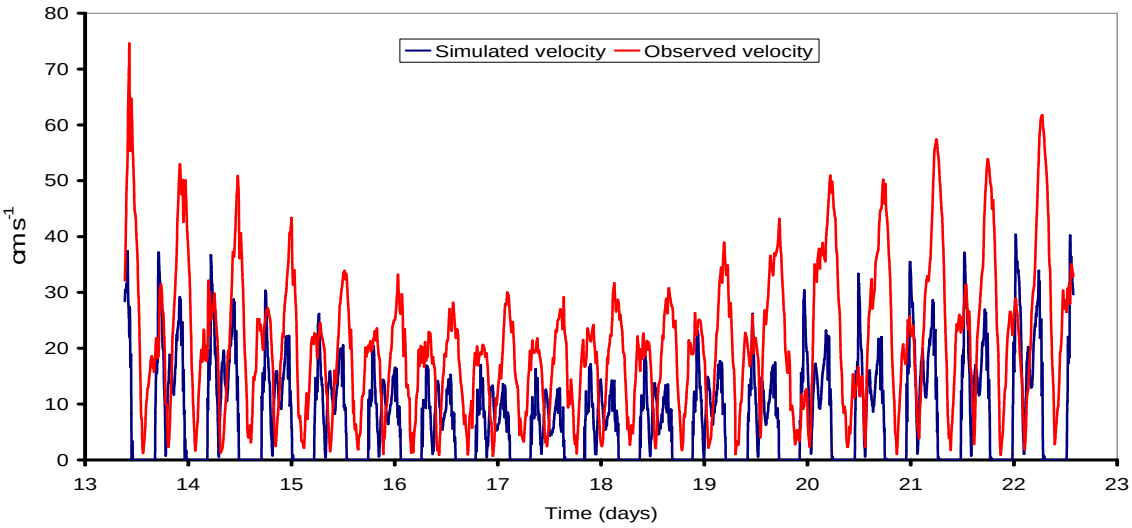

Fig. 3-5 – Predicted and measured velocities at Tavira-Cabanas (cf. – Fig. 2-4).

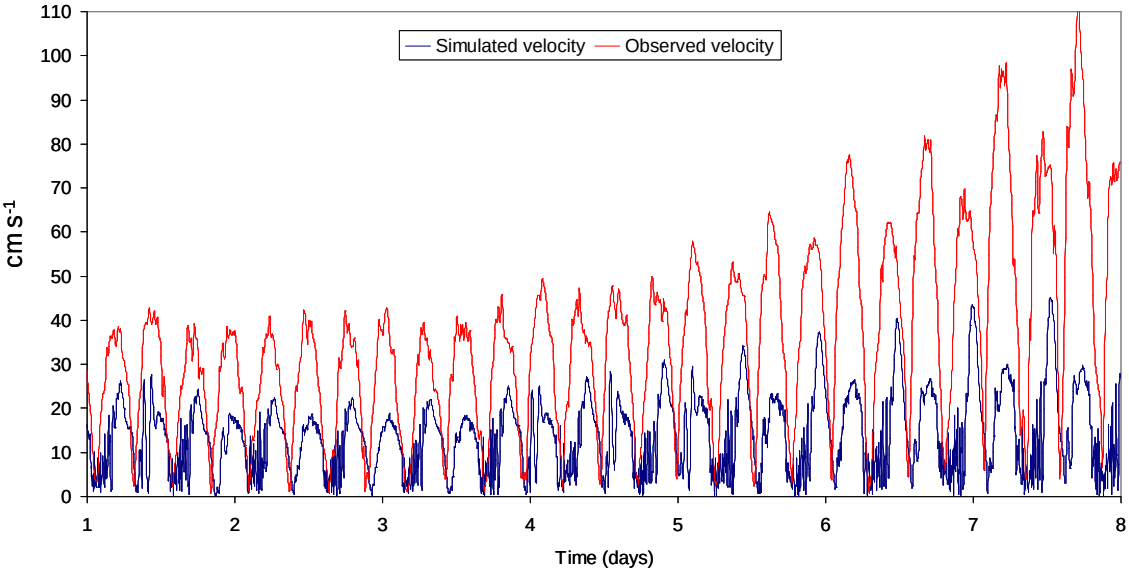

Fig. 3-6 – Predicted and measured velocities at Tavira-Clube Naval (cf. – Fig. 2-4).

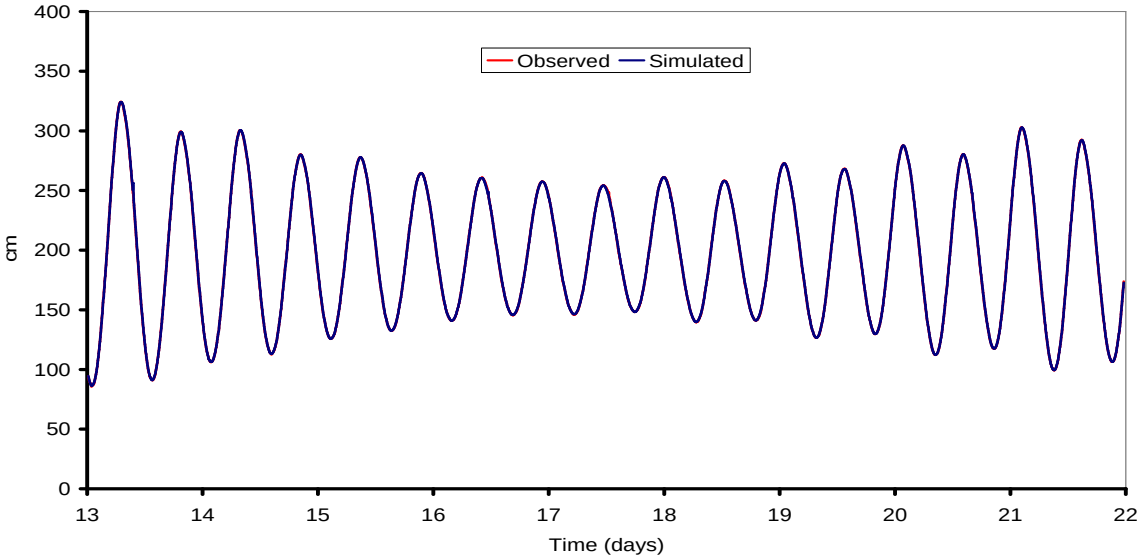

Fig. 3-7 – Predicted and measured water levels at Faro – Main Channel (cf. – Fig. 2-4).

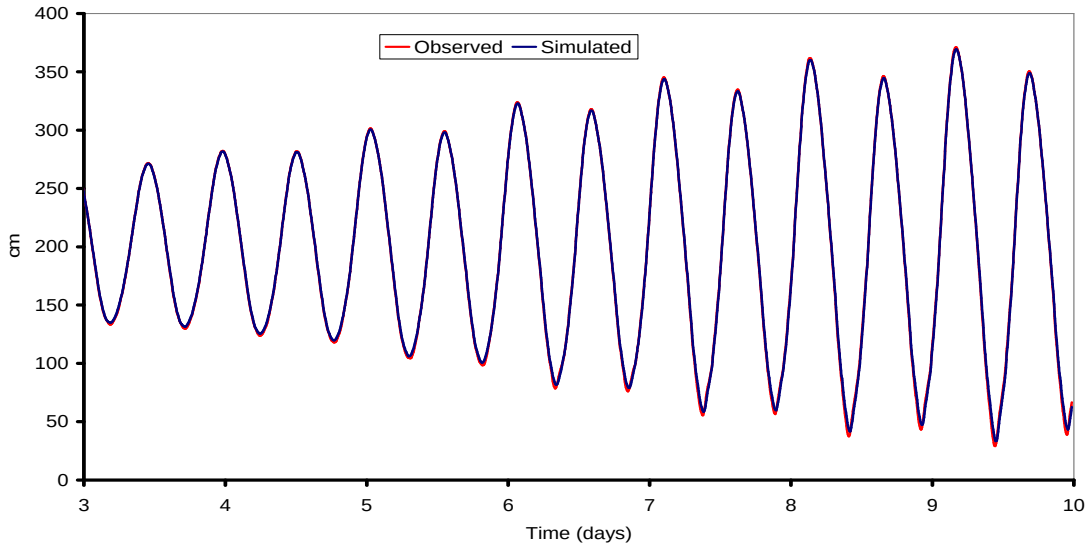

Fig. 3-8 – Predicted and measured water levels at Olhão (cf. – Fig. 2-4).

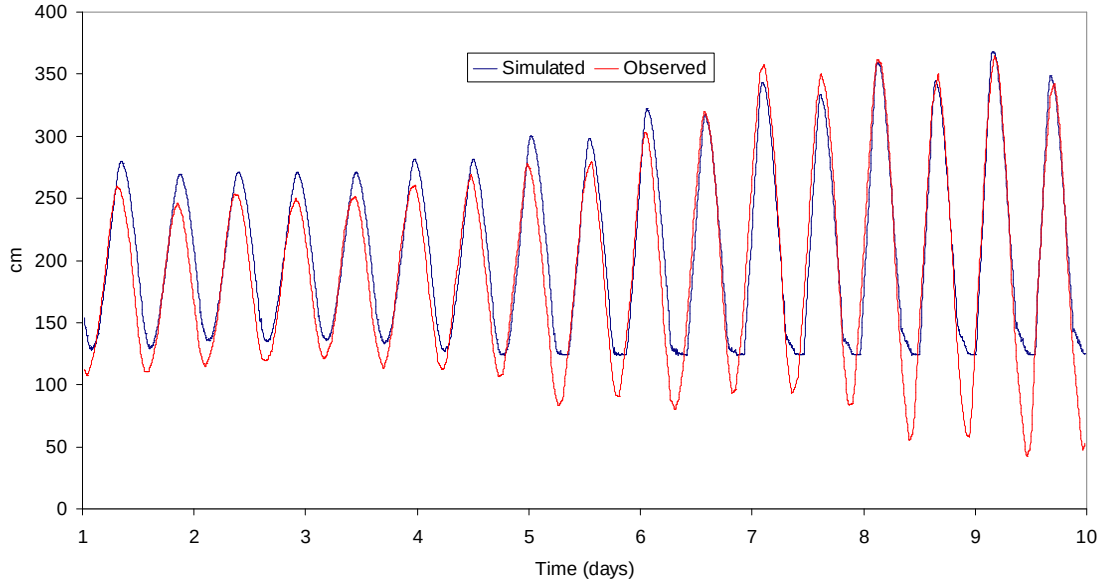

Fig. 3-9 – Predicted and measured water levels at Fuzeta - Canal (cf. – Fig. 2-4).

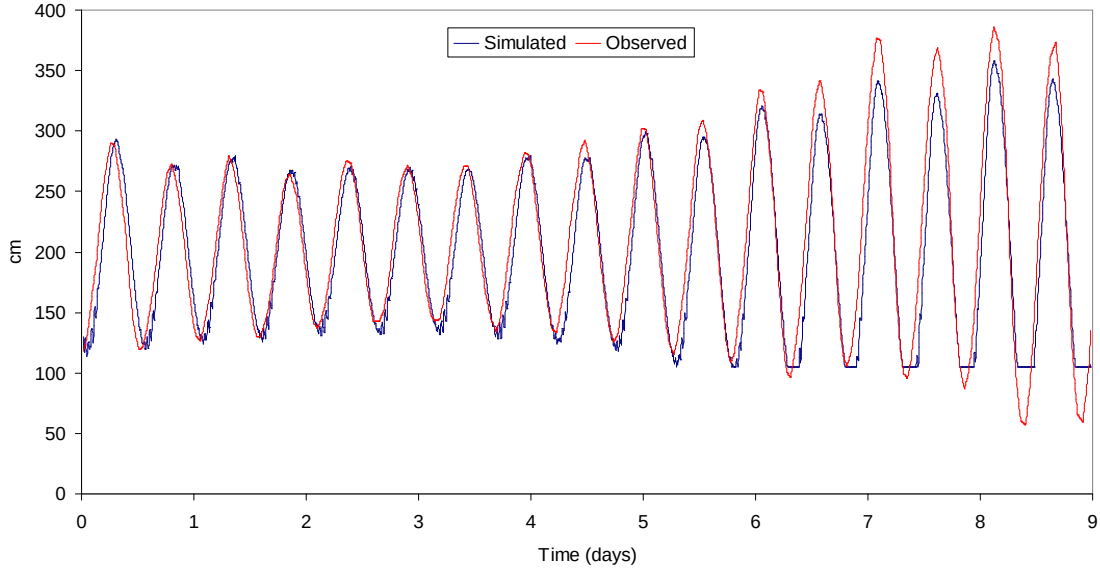

Fig. 3-10 – Predicted and measured water levels at Tavira – Clube Naval (cf. – Fig. 2-4).

The slope of the Model II regression between measured and observed values (cf. – 2.4) was s.d. from one and the y-intercept was s.d. from zero ($p > 0.05$) in almost all simulations. The variance explained by the model was significant ($p << 0.05$) in all cases. These results imply that the model explains a significant proportion of the observed variance. However, it tends to underestimate measured velocities. This may be partially explained by the relatively low model resolution (100 m, cf. – 2.2) for such a complex flow network, with many intertidal areas and narrow channels (cf. – 2.1). Furthermore, model velocity results correspond to spatially integrated values for each cell grid, whereas measurements are performed in one point in space. Therefore, it is expectable that the former tend to be smaller than the latter.

The analysis of general ebb and flood currents in Ria Formosa (Fig. 3-11) shows that there is hardly any direct flow between its western and the eastern sides, separated by a vertical line in Fig. 3-11. Therefore, it was decided to split model domain in two – a western and an eastern domain – using a higher resolution (50 m) in the latter. This splitting procedure implies important gains in computing speed, by reducing grid size from the original 282 lines and 470 columns (cf. – 2.1) to 182 lines and 300 columns, for the western sub-domain, and 69 lines and 300 columns, for the eastern sub-domain. This also allows using a larger spatial resolution in the eastern side, where more detail is needed to simulate the narrow channels and the interface with River Gilão.

The next figures (Figs. 3-12 - 3-13) include only those calibration/validation points where important changes were observed as a result of splitting model domain – Tavira-Clube Naval and Tavira-Cabanas at the “Eastern” Ria. In the former, there was an important improvement in model fit, with predicted velocities reaching higher values, closer to measurements, whereas in the latter no improvement was observed. Hereafter, the new domains will be referred as “Western” and “Eastern” Rias.

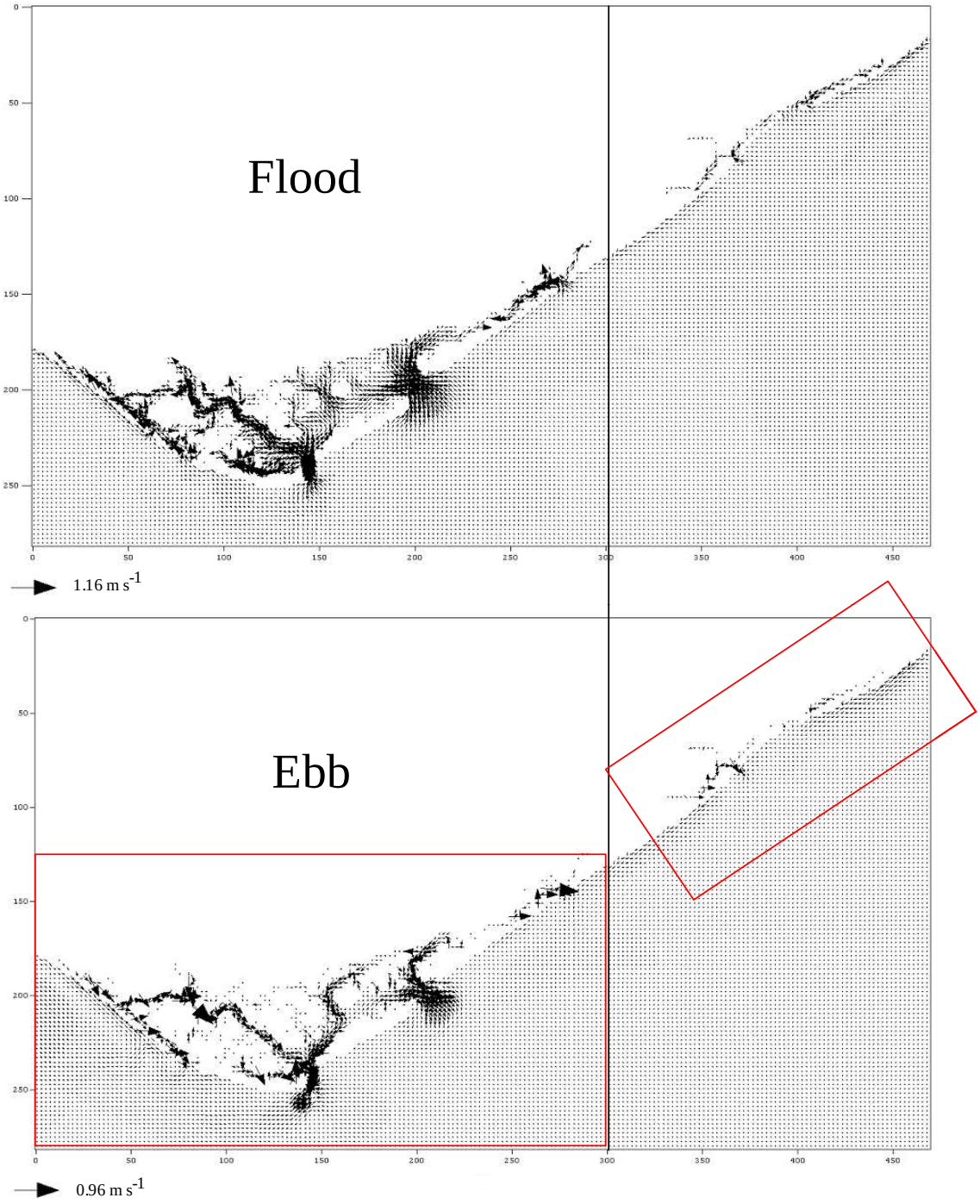

Fig. 3-11 – General circulation patterns during the flood and during the ebb. The vertical line separates the Western Ria from the Eastern Ria and the two rectangles represent the possible two sub-domains that can be considered in future simulations (see text).

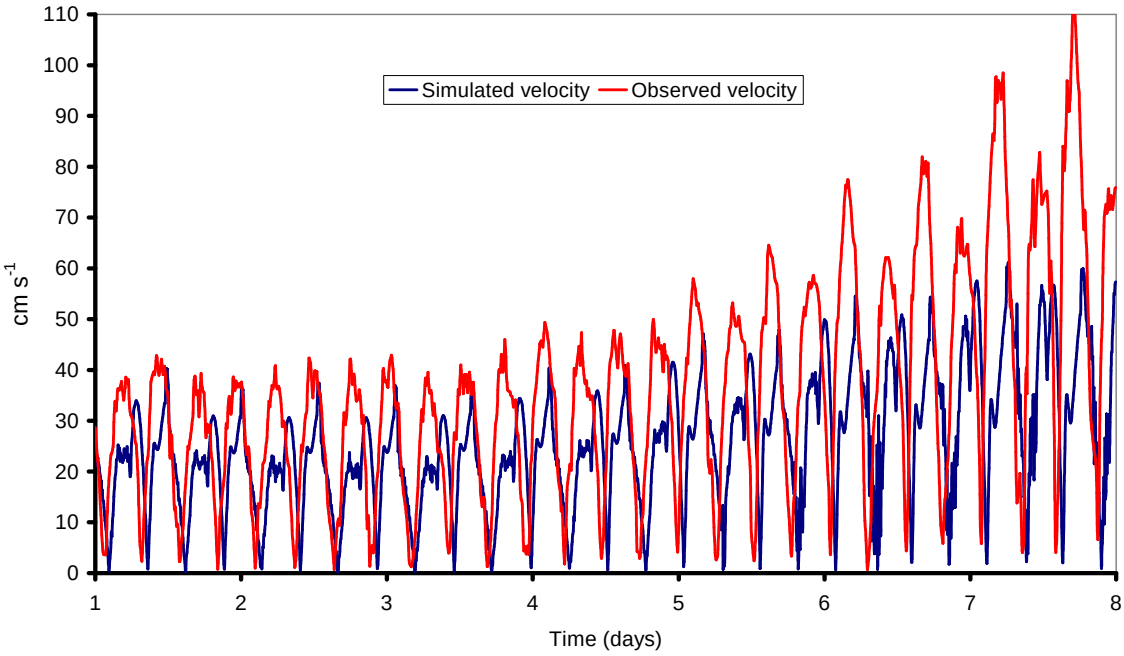

Fig. 3-12 – Predicted and measured velocities at Tavira-Clube Naval (cf. – Fig. 2-4).

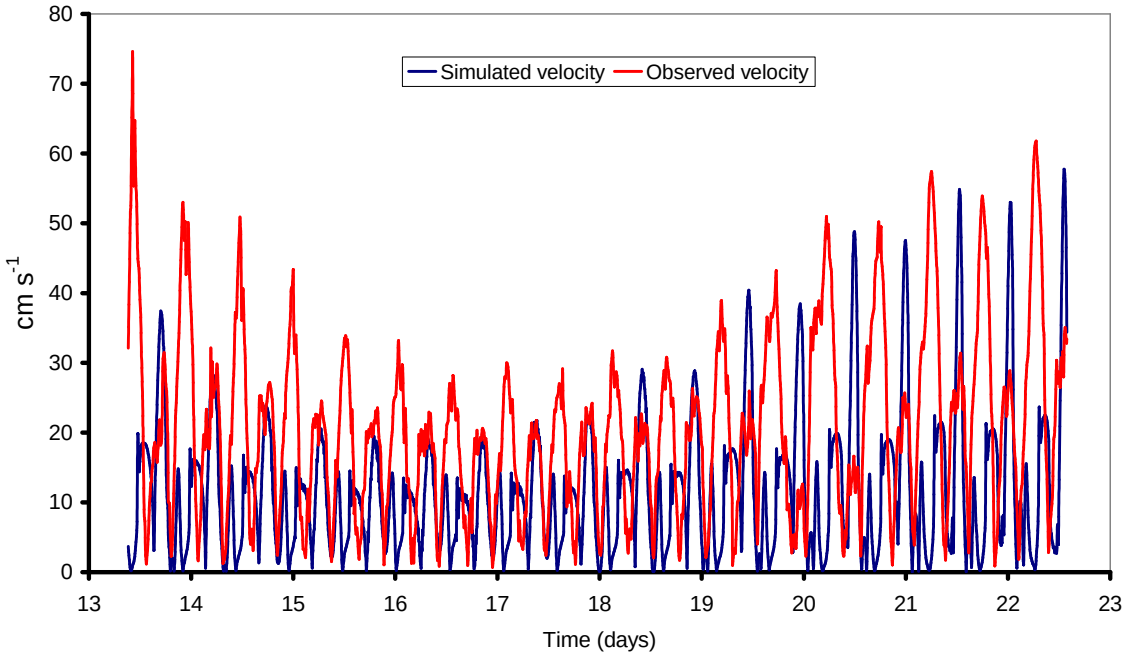

Fig. 3-13 – Predicted and measured velocities at Tavira-Cabanas (cf. – Fig. 2-4).

3.2 Analysis of general circulation patterns and residence times

General circulation patterns within Ria Formosa are shown in Figs. 3-14-3-16, during the flood and during the ebb, for the Western and the Eastern Rias. Maximum current velocities are observed at the inlets. During the ebb, water remains only in the main channels. Residual flow at the Western Ria suggests the existence of eddies near the inlets and also close to Faro-Harbour (cf. – Fig. 2-4). River Gilão, located in the Eastern Ria (Figs. 3-15 and 3-16) explains the most noticeable residual flow. A 30 m^3s^{-1} flow was used in the present simulations from rainfall-based estimates.

According to IH (2001), average ebb current velocities are higher than flood velocities for the monitoring stations depicted in Fig.2-4: Tavira-Cabanas, Tavira-Clube Naval and Olhão-Canal de Marim. The opposite is true for Fuzeta-Canal, whereas no difference was observed for the remaining two stations. These results suggest that the eastern narrow channels are ebb dominated, according to Militello & Hughes (2000).

By plotting flood currents as positive and ebb currents as negative, together with water elevations, from model data (Fig. 3-12), and calculating the flood and the ebb period, for all the current velocity monitoring stations depicted in Fig. 2-4 (Table 3-1), model results are in good agreement with the above observations regarding Tavira-Clube Naval and Fuzeta-Canal. However, the remaining sampling stations show opposite or, al least, slightly different trends, suggesting that flood dominance is the most common phenomena. The comparison of ebb and flood tidal periods, predicted by the model, confirms flood dominance, except for Faro-Harbour and Tavira-Canal (Table 3-1). According to model results, the flood period may be larger than the ebb period by nearly two hours in Ancão, Fuzeta-Canal and Tavira-Cabanas. These patterns may be explained by flow divergence (see below).

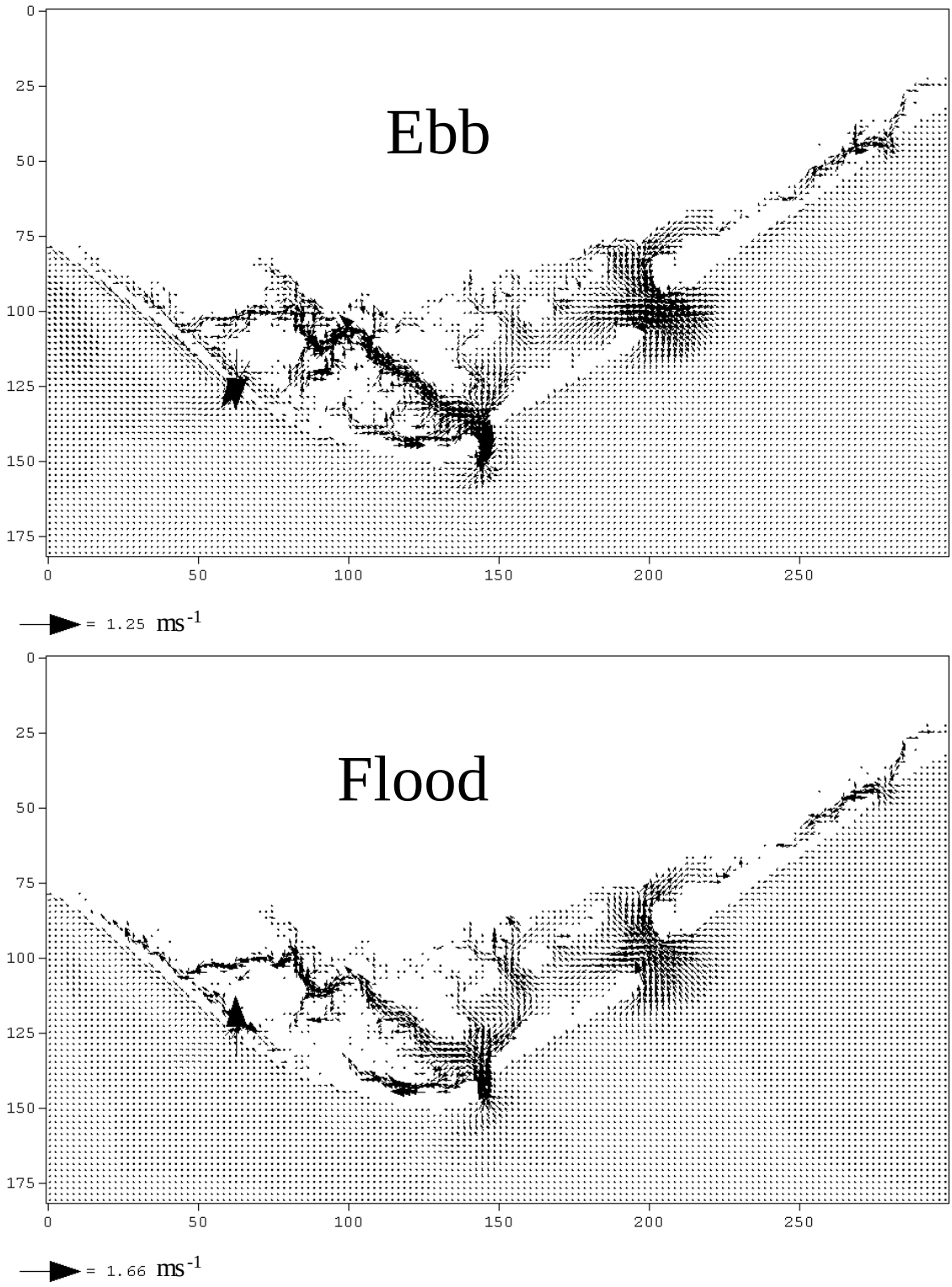

Fig. 3-14 – General circulation patterns during the ebb and during the flood at the Western Ria (see text).

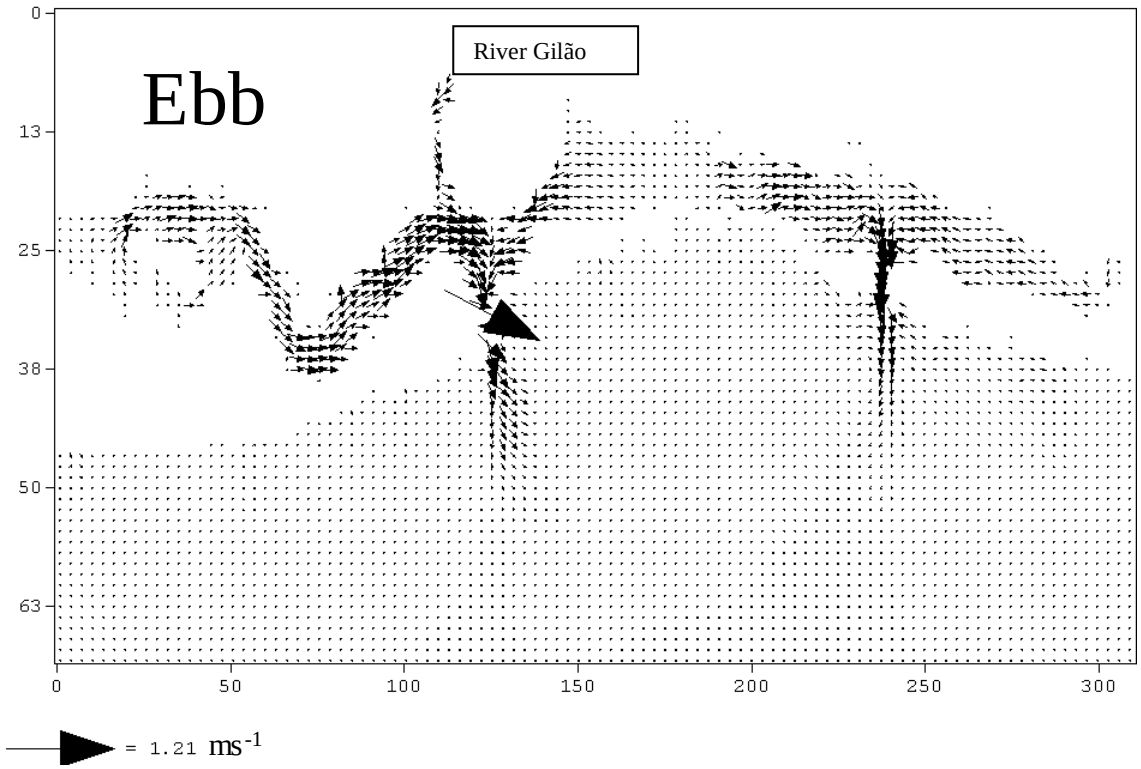

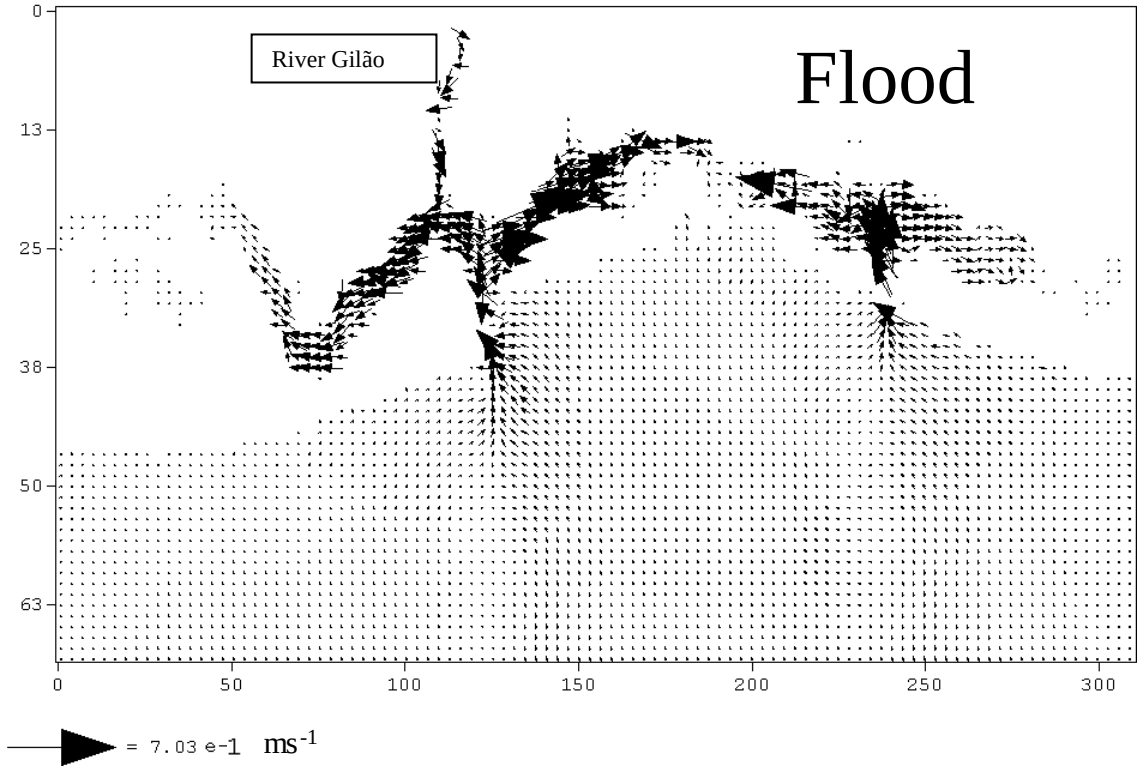

Fig. 3-15 – General circulation patterns during the ebb and during the flood at the Eastern Ria (see text).

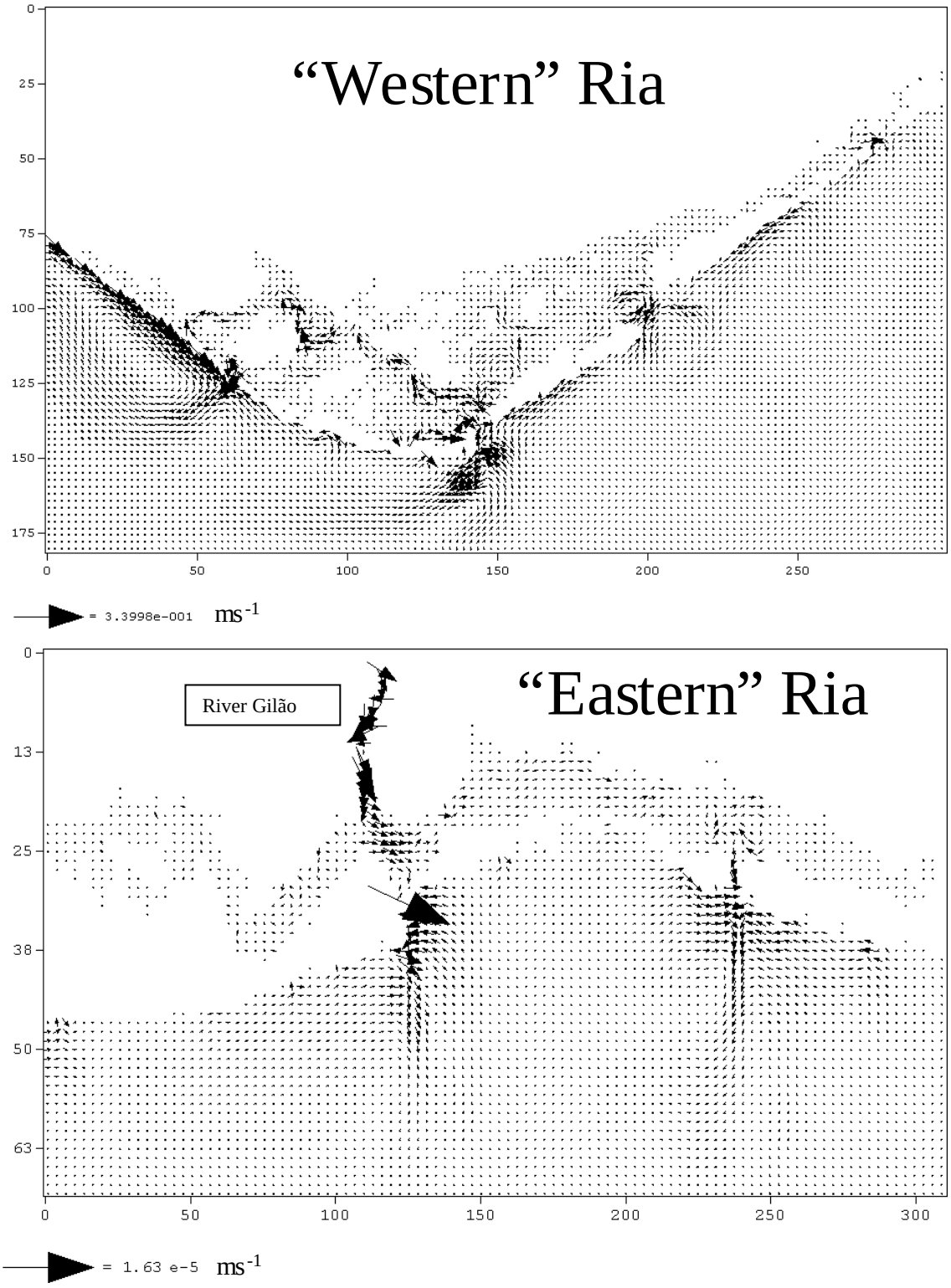

Fig. 3-16 – Residual flows at the Western and the Eastern Rias (see text).

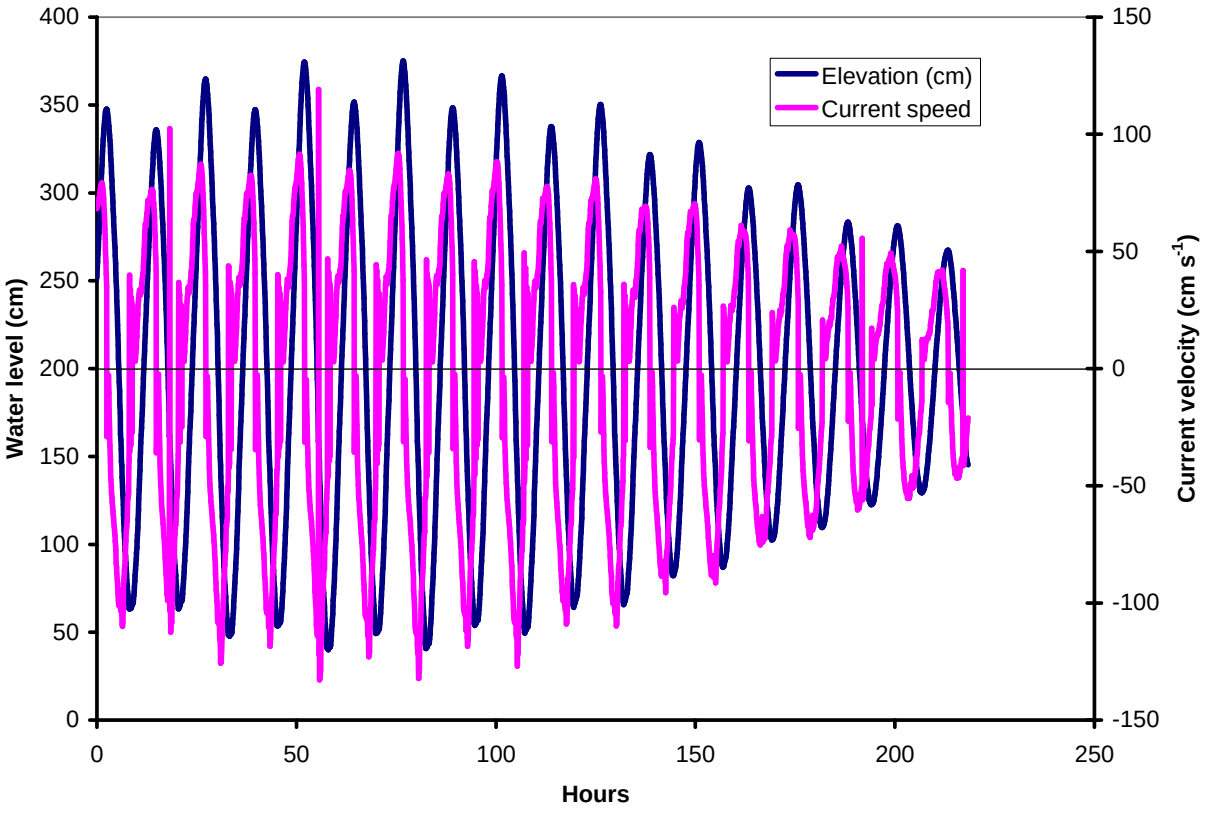

Fig. 3-17 – Measured water levels and current velocities at Fuzeta-Canal (cf. – Fig. 2-4). Flood and ebb velocities plotted as positive and negative, respectively (see text).

Table 3-1 – Predicted average ebb and flood current velocities and periods at the current meter stations depicted in Fig. 2-4 (see text).

Station	**Ebb**		**Flood**	
	Average current velocity (cm s^{-1})	Period (h)	Average current velocity (cm s^{-1})	Period (h)
Ancão	17.90	7.16	24.57	5.20
Faro-Harbour	50.69	6.10	39.49	6.06
Olhão-Canal de Marim	32.30	6.72	31.07	5.47
Fuzeta-Canal	28.49	6.25	37.92	4.94
Tavira-Clube Naval	38.56	6.16	33.25	6.16
Tavira-Cabanas	10.20	6.90	15.38	4.81

The integration of flows across the inlets made possible to estimate their average input-output values for a period of a month. In Fig. 3-18, a synthesis of obtained results over the whole Ria shows that the Faro-Olhão inlet is by far the most important, followed by Armona, Tavira, "new", Cabanas and Fuzeta inlets. It is also apparent that the Faro-Olhão has a larger contribution as an inflow pathway, whereas the remaining ones contribute more as outflow pathways. The difference in input and output flows over the integration period was a 114 m^3s^{-1}input, for the Western Ria, and a 46 m^3s^{-1}output, for the Eastern Ria.

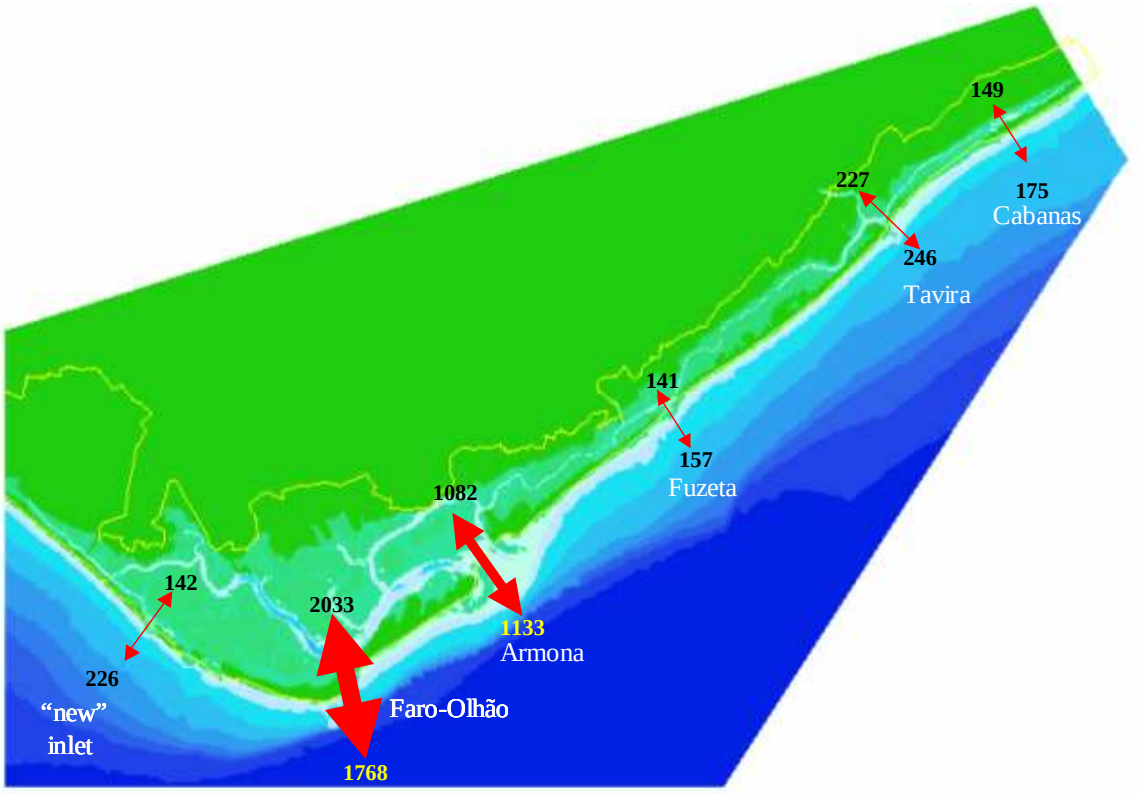

Fig. 3-18 – Averaged inflows and outflows (m3 s-1) through Ria Formosa inlets (see text).

The above results do not imply any violation of volume conservation, but solely that during the period considered there was a net exchange of volume between the Ria and the sea, on the western side, and also between River Gilão and the Ria, on the eastern side. The results obtained suggest that part of the water that enters the Ria though the Faro-Olhão inlet is distributed west and eastwards (cf. Fig. 3-14), probably reducing the flood period in other areas as referred above for Ancão and Fuzeta (cf. Table 3-1). At the Eastern Ria, part of River Gilão water outflows though Tavira inlet, but part is diverted towards Cabanas (cf. Fig. 3-15), probably reducing the flood period eastwards (cf. Table

3-1). The results presented in Table 3-1 suggest that flood period is larger or equals the ebb period. This may result from ebb water taking more time to reach the ocean by outflowing only thought nearby inlets, whereas during the ebb, there seems to some volume redistribution among different inlets.

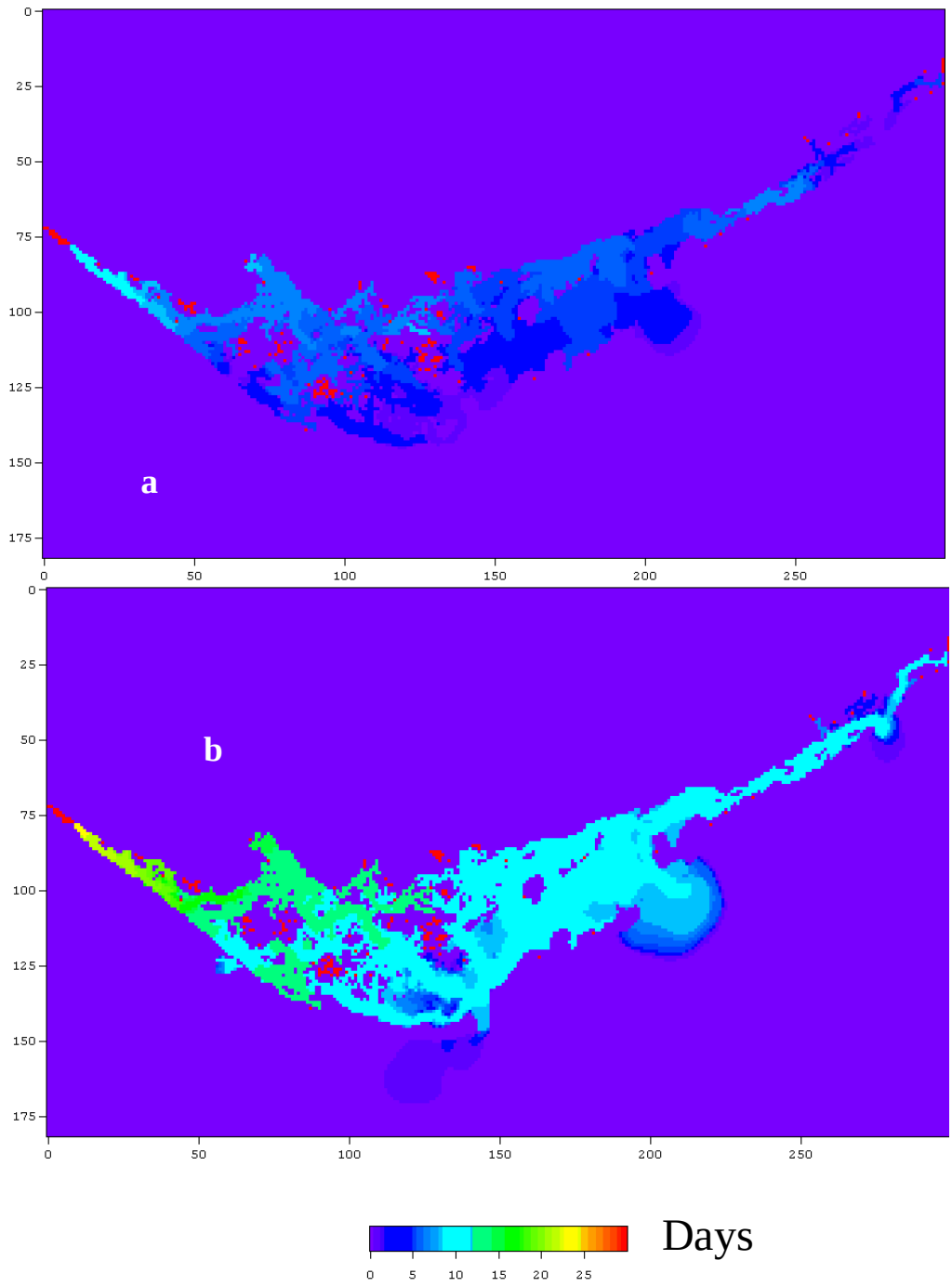

Fig. 3-19 – Half residence time (a) and time for 90% washout (b) of Western Ria water (see text).

Figs. 3-19 and 3-20 show the estimated half residence and the time for the washout of 90% of lagoon water (cf. – 2.4). As expected, areas located near inlets have relatively small residence times, of less than five days, for the removal of 90% of their water, whereas inner areas, may have a half residence time of over two weeks. This is more evident in the Eastern Ria, due of its narrow inlets.

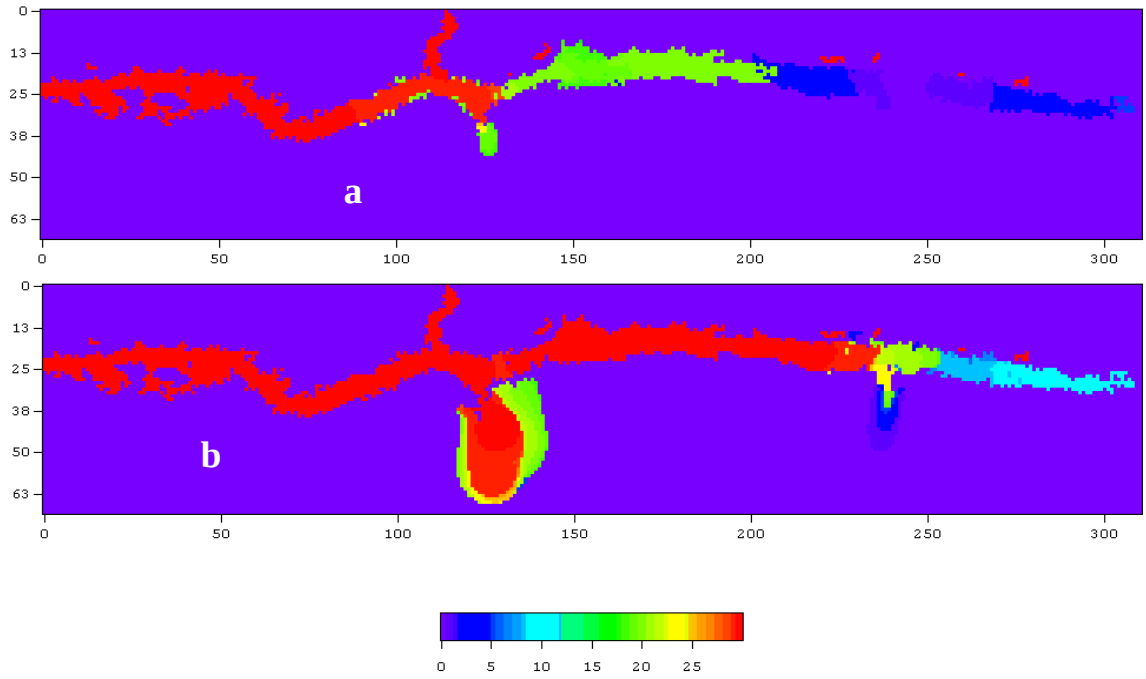

Fig. 3-20 – Half residence time (a) and time for 90% washout (b) of eastern lagoon water (see text).

3.3 Dilution of effluents from Waste Water Treatment Plants

Figs. 3-21 and 3-22 show the concentration decay of the tracer introduced through the Northwest Faro and Fuzeta WWTPs, and through the East and West Olhão WWTPs, respectively (cf. – 2.7). For comparison purposes, a reference concentration of 0.005 concentration units was assumed. From these figures it is apparent that the WWTP location exhibiting a faster decay, among those analysed, is the West Olhão WWTP. The semi-diurnal tidal harmonic effect over concentration, at the discharge point is more visible for this WWTP than for the remaining ones.

Figs. 3-23 and 3-24 show the evolution of the conservative tracer concentration released from the Northwest Faro WWTP and its dispersion through the lagoon channel after 2, 10 and 40 and 120 hours of simulation, respectively. During the first hours, the tracer disperses to the sea through the main channels, but as the simulation approaches the end, part of the tracer gets trapped in the inner western channels.

Main soil uses in the surroundings of the WWTPs are depicted in Fig. 3-25. For example, the Northwest Faro WWTP discharge point is located in a fishpond area, suggesting a high degree of sensitivity to effluent discharges. There are also salt marshes in this area, which enhance the ecological significance of the place. In other zones such as the West Olhão WWTP, there are shellfish growing areas, the quality of which is compromised by bacterial contamination. Furthermore, episodes of high shellfish mortalities have occurred in these areas.

The results presented here are not an exhaustive analysis of the WWTPs effluent dispersion, but just an example of the work that is being developed within the DITTY project. In a future report, these issues will be the subject of an in depth analysis, considering not only the current WWTPs, but also the planned ones for the near future. Furthermore, numerical experiments will be carried out with conservative and non-conservative tracers.

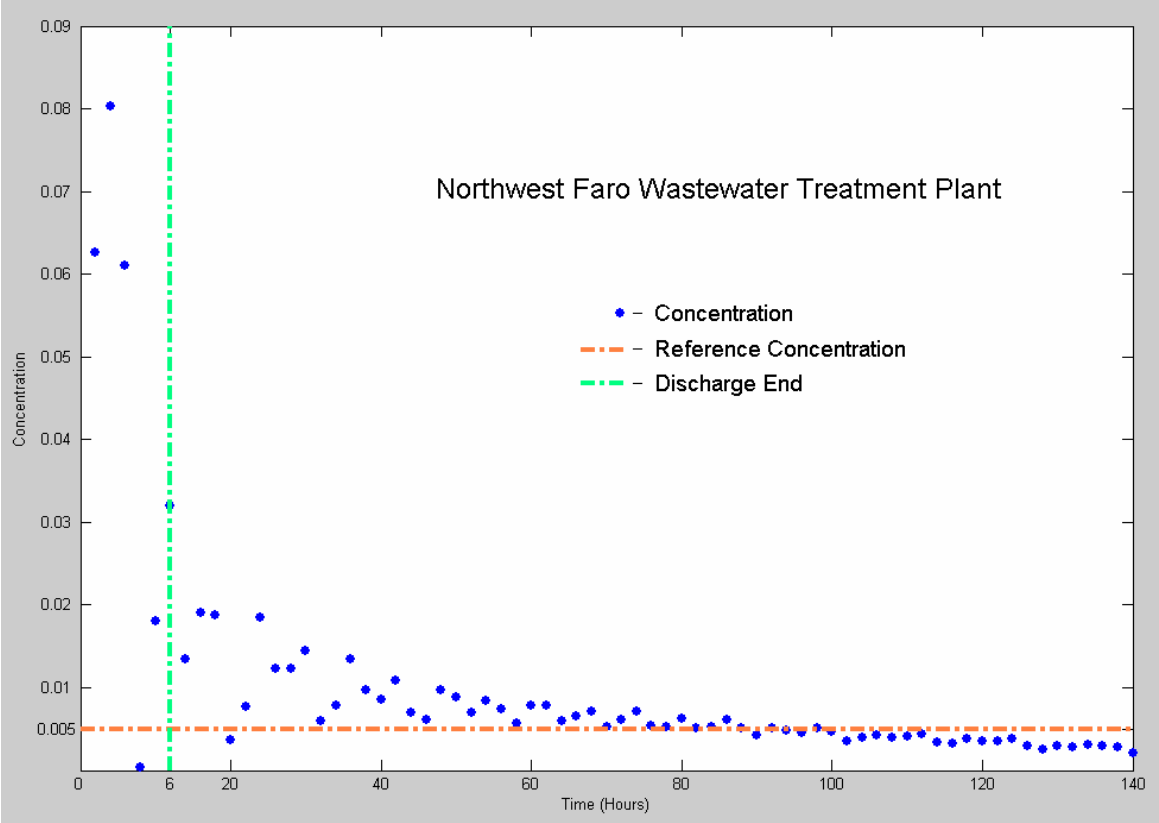

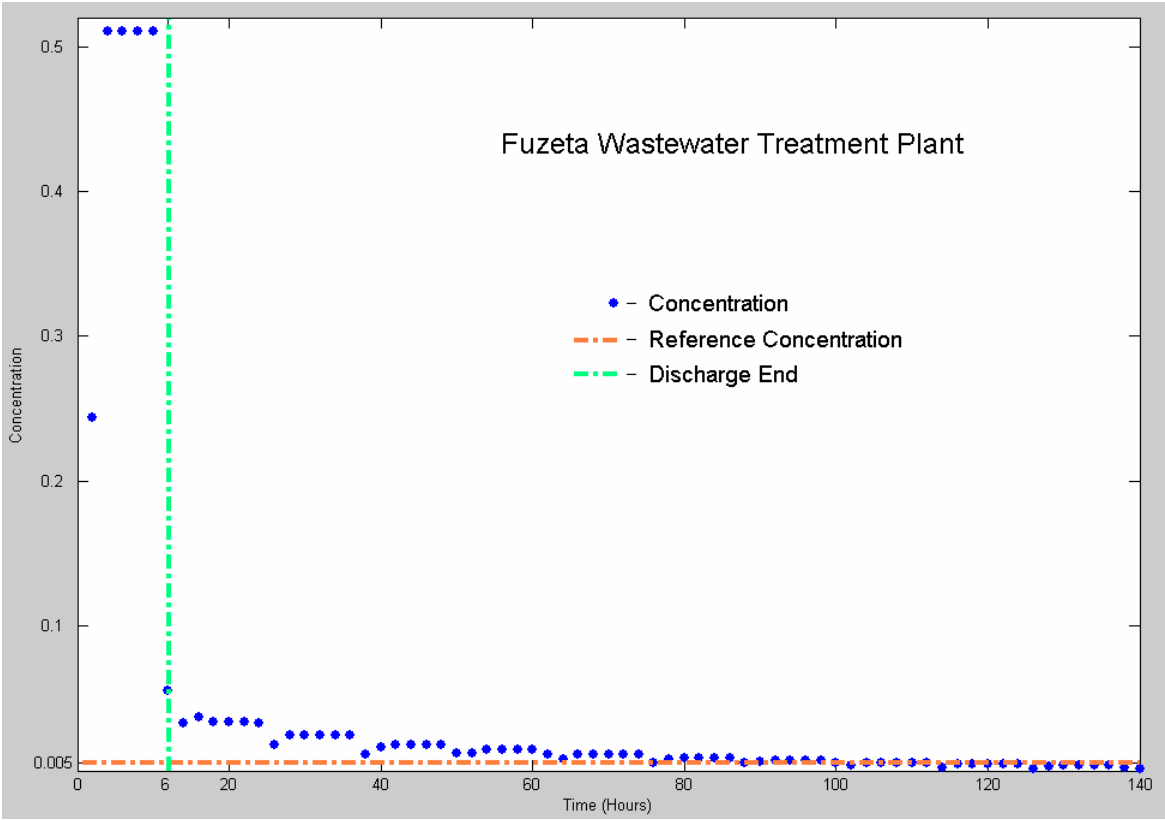

Fig. 3-21 – Tracer decay curves for the Northwest Faro and Fuzeta WTP's.

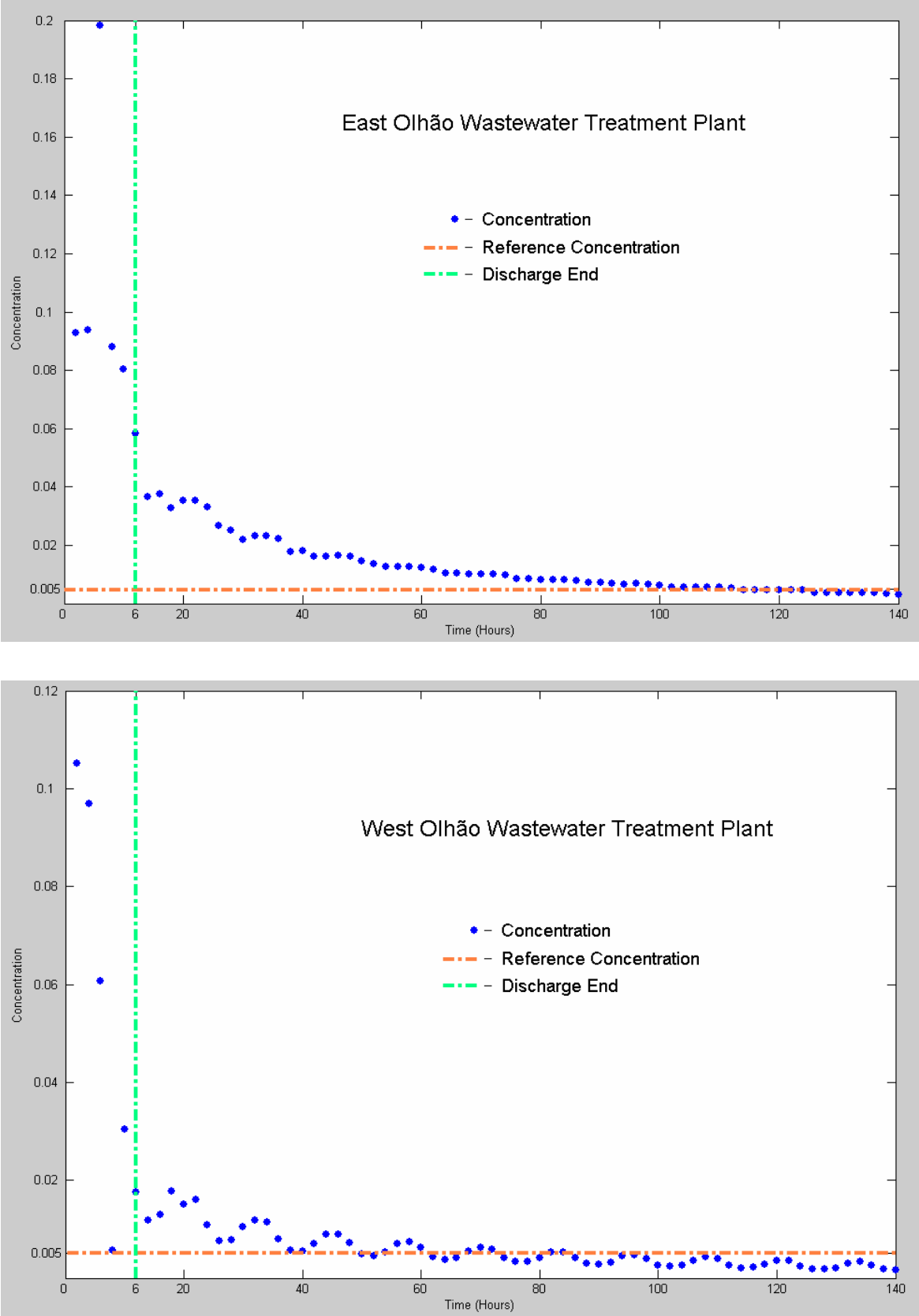

Fig. 3-22 – Tracer decay curves for the East and West Olhão WTP's.

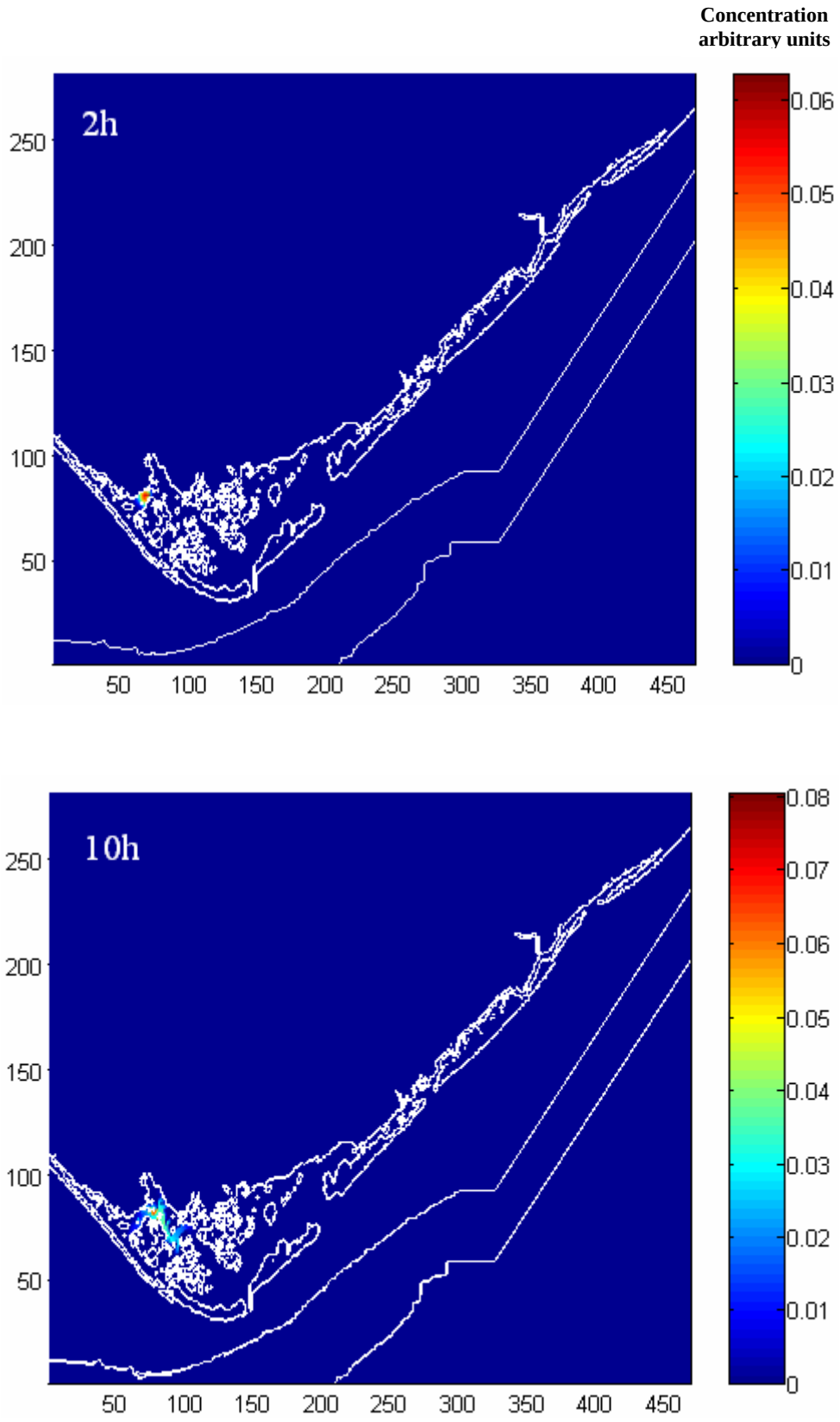

Fig. 3-23 – Tracer concentration two and ten hours after the beginning of the simulation (Northwest Faro WWTP) (see text).

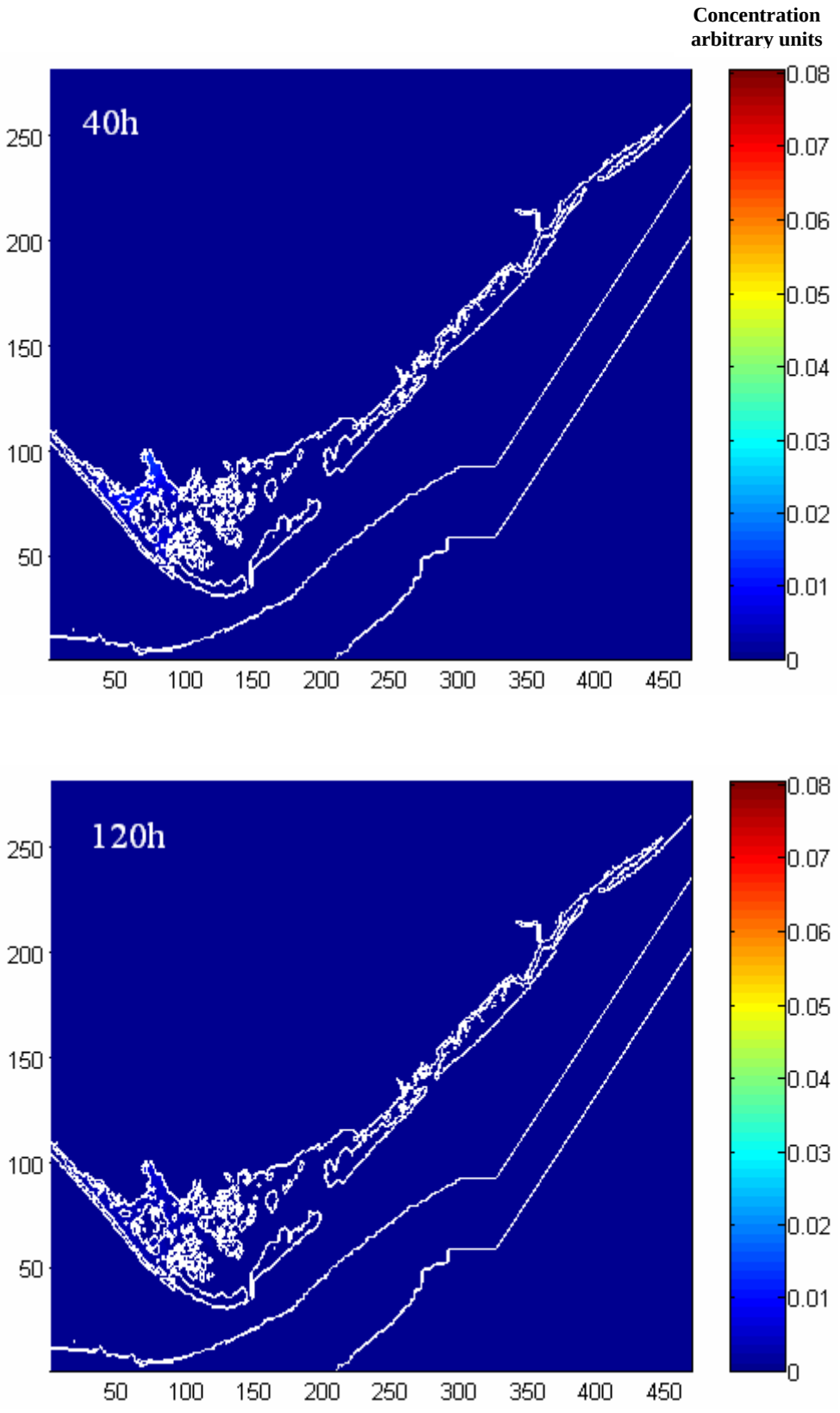

Fig. 3-24 – Tracer concentration 40 and 120 hours after the beginning of the simulation (Northwest Faro WWTP) (see text).

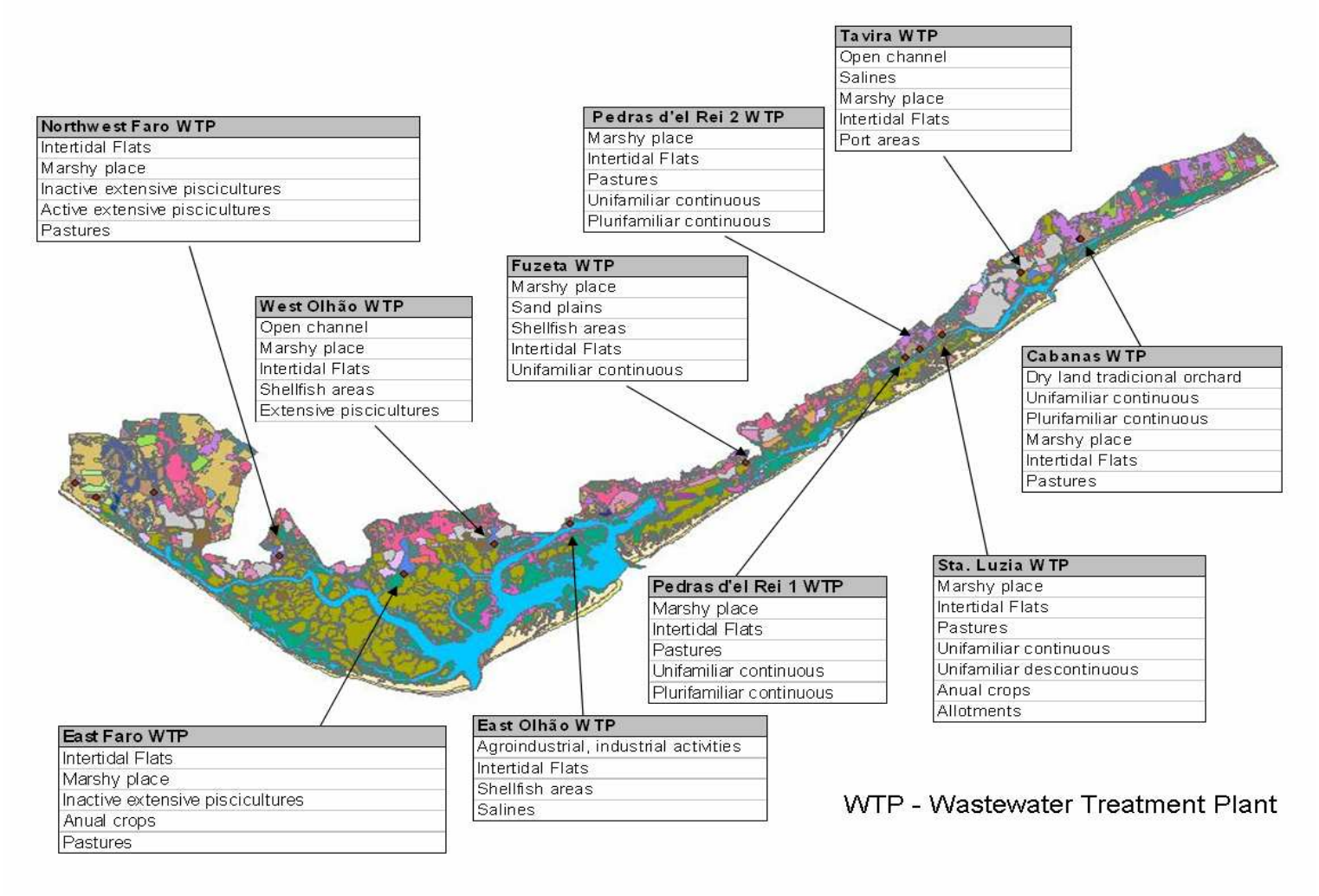

Fig. 3-25 – Soil use in the surroundings of the analysed WWTPs.

4 Conclusions

The hydrodynamic model presented in this report has been compared with real data. The visual fit of the model looks quite good for the majority of monitoring stations, both in terms of current velocities and water levels. The statistical analysis based on Model II regression between measured and simulated results shows that the model explains a significant amount of system variability. However, it tends to underestimate current velocities. This underestimation may be justified by spatial integration of model predictions (100 m) compared with the current velocity measurements, undertaken at one point in space. Since no efforts were carried out to tune the model results towards observations, it is reasonable to assume that the model appears to be reasonably validated.

The model was used to analyse general circulation patterns in Ria Formosa, showing the dominant contribution of the Faro-Olhão and Armona inlets for the lagoon-sea water exchanges and the variability in water residence time at different areas of the lagoon.

Some simulations were also carried out to simulate the dispersion of conservative tracers from the WWTP. The obtained results will be useful to understand the location effects of the WWTPs in the dilution time of their effluents.

5 References

1) Pereira, A. & P. Duart, 2005. EcoDynamo Ecological Dynamics Model Application. University Fernando Pessoa.

2) Falcão, M, Fonseca, L., Serpa, D., Matias, D., Joaquim, S., Duarte, P., pereira, A., Martins, C. & M.J. Guerreiro, 2003. Synthesis report. EVK3-CT-20022-00084 (DITTY Project).

3) Instituto Hidrográfico (IH), 2001. Proj. OC4102/01, Maria Formosa, Relatório Técnico Final, Rel. TF. OC 04/2001, Monitorização Ambiental. Instituto Hidrográfico, Divisão de Oceanografia.

4) Laws, E.A., Archie, J.W., 1981. Appropriate use of regression analysis in marine biology. Marine Biology 65, 99 – 118.

5) Mesplé, F., Trousselier, M., Casellas, C. & P. Legendre, 1996. Evaluation of simple statistical criteria to qualify a simulation. Ecological Modelling 88, 9 – 18.

6) Press, W.H., Teukolsky, S.A., Vetterling W.T. & B.P. Flannery, 1995. Numerical recipes in C - The art of scientific computing. Cambridge University Press, Cambridge.

7) Militello, A. & S.A. Hughes, 2000. Circulation patterns at tidal inlets with jetties. US Army Corps of Engineers.

8) Neves, R.J.J., 1985. Étude expérimentale et modélisation mathématique des circulations transitoire et rédiduelle dans l'estuaire du Sado. Ph.D. Thesis, Université de Liège.

9) Service Hydrographique et Océanographique de la Marine (SHOM), 1984. Table des marées des grands ports du Monde. Service Hydrographique et Océanographique de la Marine, 188 pp.

10) Sokal, R.R. and F.J. Rohlf, 1995. Biometry, The principles and practise of statistics in biological research. W.H. Freeman and Company, 887 pp.

11) Vreugdenhil, C.B., 1989. Computational hydraulics, An introduction. Springer-Verlag, 183 pp.

12) UE (2000). Directiva 2000/60/CE do Parlamento Europeu e do Conselho que estabelece um Quadro de Acção Comunitária no Domínio da Política da Água. J.O.C. de 22.12.2000.